The effect of dark matter capture on binary stars

Daniel Carrera

Lund Observatory
Lund University

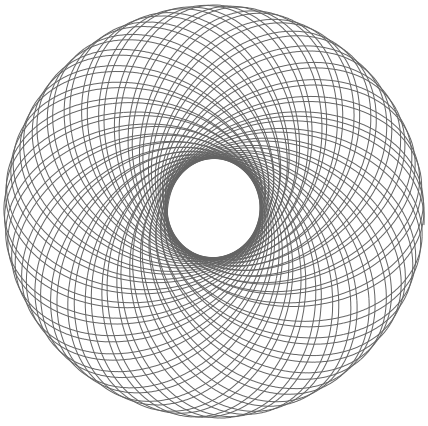

2012-EXA63

Degree project of 60 higher education credits (for a degree of Master)
May 2012

Lund Observatory
Box 43
SE-221 00 Lund
Sweden

Lund Observatory, Sweden

The effect of dark matter capture on binary stars

Masters Thesis

Daniel Carrera

Supervisor: Dr Ross Church

14 May 2012

Abstract

WIMPs, or Weakly Interacting Massive Particles, are a popular dark matter candidate, but their detection remains elusive. At its core, this project is an effort to bridge the gap between the theory of WIMPs, and astronomical observation.

According to the WIMP model, stars in the galaxy travel through a background field of WIMPs that are constantly crossing the star. Some of these WIMPs collide with atomic nuclei inside stars via the weak force interaction. The ones that lose sufficient kinetic energy become bound to the star. Captured WIMPs gradually accumulate inside the core of the star, where they annihilate with each other. This converts the entire WIMP mass into energy. A star that captures a significant number of WIMPs could receive most of its energy from WIMP-WIMP annihilation. This would have dramatic effects in the star's structure and evolution, greatly prolonging its life. The possibility of directly observing stars powered by WIMP annihilation is the driving force behind this project.

In this project I have modelled collisions between WIMPs and atomic nuclei, via the weak interaction. Combined with an N-body simulation, I have been able to model WIMP capture in both single stars and binary systems. This work has led to a number of interesting conclusions: (1) Binary stars, due to their orbital motion, can produce more collisions that result in initially bound orbits. However, the gravitational interaction with two masses quickly scatters nearly all WIMPs out of the system. The few that survive, end up in rosette-shaped orbits that do not pass through either star. As a result, the WIMP capture rate in binaries is essentially zero. (2) These semi-stable rosette orbits mean that stars in a binary are surrounded by *WIMP halos*, with a much higher density than the background. These halos will be a source of gamma ray radiation as WIMPs collide and annihilate. Unfortunately, the resulting WIMP flux at the Earth is merely 4×10^{-5} photons $\mathrm{m}^{-2}\,\mathrm{yr}^{-1}$ even in the most optimistic scenario. (3) Lastly, it is highly unlikely that any WIMP-burning star (single or in a binary) can be found anywhere in our galaxy.

Swedish Summary

Det är numera allmänt vedertaget att 80% av materian i universum består av en ny sorts partiklar som inte strålar eller interagerar med ljus. Med andra ord, den är ”mörk”. Vi känner redan till en slags ”mörk” partikel - neutrinon. Alla partiklar som är elektriskt oladdade är ”mörka”, men mörk materia kan inte huvudsakligen bestå av neutriner. Mörk materia verkar bestå av partiklar som är mycket mer massiva än några andra partiklar man känner till idag - runt 100 gånger protonens massa.

Eftersom mörk materia inte interagerar med ljus är den väldigt svår att upptäcka och studera. Alla försök att upptäcka mörk materia förlitar sig på idén att den fortfarande kan interagera med vanlig materia på andra sätt. Framförallt att mörk materia kan kollidera med vanliga partiklar. Det finns många experiment över hela världen där man försöker upptäcka de här kollisionerna, men än så länge har inget av dem lyckats.

Det här projektet är ett försök att utveckla ett annat sätt att upptäcka mörk materia, nämligen genom att undersöka dess effekt på dubbelstjärnor. När partiklar av mörk materia kolliderar med väteatomer inuti en stjärna förlorar de fart och kan bli fångade av stjärnans gravitation. Om en stjärna samlar på sig tillräckligt mycket mörk materia kan det ändra stjärnans struktur på ett observerbart sätt. T.ex. skulle partiklar av mörk materia troligtvis förstöras genom annihilation mellan materia och antimateria och därmed bidra med energi till stjärnan. Denna extra energikälla skulle tillåta en stjärna att leva, i princip, för evigt. Den här sortens stjärnor, drivna av mörk materia, skulle man kunna känna igen om man såg dem genom ett teleskop.

Jag har använt datorsimuleringar för att göra modeller av hur dubbelstjärnor fångar in mörk materia. Problemet är komplicerat eftersom gravitationen från de två stjärnorna skapar komplicerade banor för partiklarna. Tyvärr visar mina resultat att dubbelstjärnor fångar in ännu mindre mörk materia än vad ensama stjärnor gör. Dessutom, även under de mest optimistiska förhållandena finns det antagligen inte några stjärnor i vår galax som har samlat in tillräckligt mycket mörk materia för att det ska ge en synbar effekt.

Contents

Chapter 1

Introduction

1.1 Motivation

According to the current ΛCDM model of cosmology, 23% of the universe is made of some mysterious substance called Dark Matter. The most popular candidate for dark matter is a hypothetical particle called a WIMP (Weakly Interacting Massive Particle). WIMPs have a strong theoretical motivation, but their detection remains elusive.

The motivation behind this thesis is the desire for a practical observational test that can determine whether dark matter is indeed made of WIMPs.

It may be possible to use observations of stellar binaries to either detect the presence of WIMPs through a means other than gravity, or to impose new constraints on the WIMP interaction cross section.

1.2 Dark matter

The first evidence for unseen matter in the universe came as early as 1933, when Zwicky (1933) applied the virial theorem[1] to the Coma galaxy cluster and inferred the existence of large amounts of unseen mass.

Additional evidence had to wait almost 40 years, when Vera Rubin began studying the rotation curve of M31 (Andromeda Galaxy), shown in Figure 1.1. As is typical for a spiral galaxy, the star light (and hence, the visible mass) of M31 is concentrated in a small bulge at the centre of the disk. If this is correct, then outside the bulge the gravitational potential should resemble a point-mass potential, meaning that the speed of stars around the galaxy should approximately follow the relation:

$$v_{orb} = \sqrt{\frac{G\,M}{R}}$$

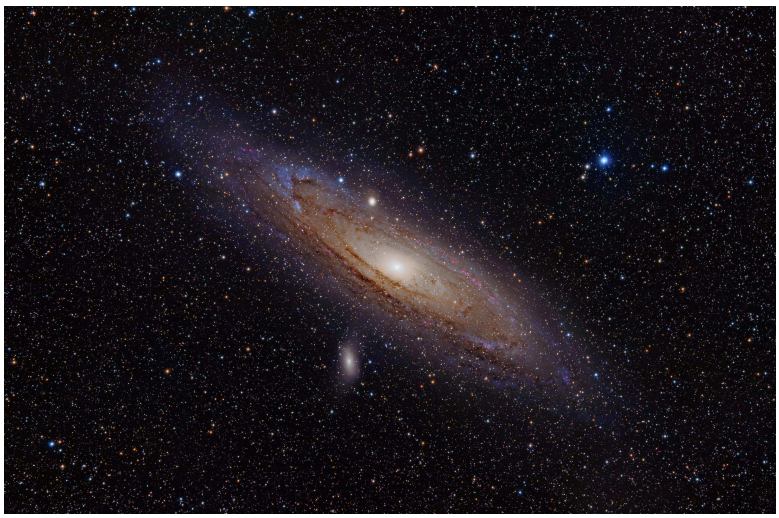

Figure 1.1: Amateur photograph of M31 by Evans (2010). Most of the visible matter (star light) is concentrated in a small bulge at the centre of M31. The outer part of the galaxy looks bright due to the presence of very bright blue stars. With most of the mass concentrated at the centre, the speed of stars around the galaxy should drop approximately as $v_{orb} \sim R^{-1/2}$.

Instead of a $v_{orb} \sim R^{-1/2}$ law, Rubin & Ford (1970) reported a relatively flat rotation curve along the spiral arms (Figure 1.2), indicating that the mass of M31 increases linearly with distance to the centre (Rubin & Ford, 1970).

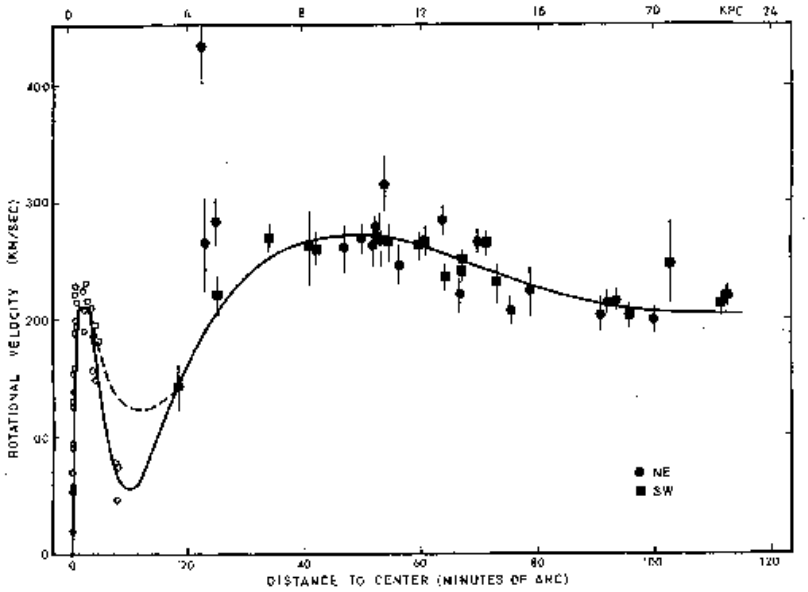

Figure 1.2: Original figure by Rubin & Ford (1970) showing the galaxy rotation curve of M31. The flat velocity curve away from the galactic centre indicates that M31's potential does not resemble a point mass potential. The galaxy mass grows linearly with distance to the centre, indicating the presence of vast amounts of unseen mass.

Today the evidence is overwhelming that we live in a universe comprised of about 4.6% baryonic matter, 23% dark matter and 72% dark energy. In addition to galaxy clusters and galaxy

[1]The virial theorem relates the mean kinetic energy $\langle T \rangle$ and potential energy $\langle V \rangle$ of a system of particles bound by a potential: $2\langle T \rangle = -\langle V \rangle$

rotation curves, we now have a great deal of cosmological evidence from the Cosmic Microwave Background (CMB), Baryon Acoustic Oscillations (BAO) and Type Ia supernovae (Figure 1.3). Astronomers normally express the mass density of the universe as the quantities Ω_M and Ω_Λ:

$$\Omega_M = \frac{\text{Mass density of matter}}{\text{Critical density}} = \frac{\rho_M}{\rho_{crit}} \qquad \Omega_\Lambda = \frac{\text{Mass density of ``dark energy''}}{\text{Critical density}} = \frac{\rho_\Lambda}{\rho_{crit}}$$

Where the critical density ρ_{crit} is the energy density needed to give a flat universe. In other words, if $\Omega_M + \Omega_\Lambda = 1$, we live in a universe with zero global curvature. As Figure 1.3 shows, modern observations paint a picture of a universe with $\Omega_\Lambda \approx 0.72$ and $\Omega_M \approx 0.28$ (see e.g. Amanullah et al., 2010). This much matter is inconsistent with Big Bang nucleosynthesis unless most of this matter is non-baryonic (Olive et al., 2000; Taoso et al., 2008). This immediately discards brown dwarfs and compact objects (e.g. neutron stars) as candidates for the missing matter.

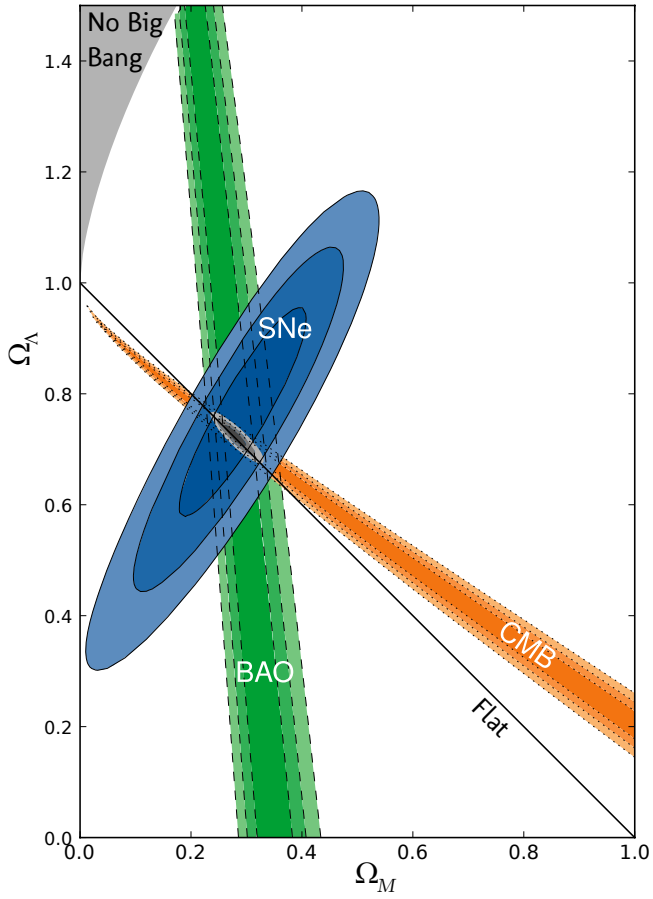

Figure 1.3: This graph shows how the data from Type Ia supernovae (blue), the Cosmic Microwave Background (orange) and Baryonic Accoustic Oscillations (green) all intersect at a point consistent with $\Omega_\Lambda \approx 0.72$ and $\Omega_M \approx 0.28$ (see text for a description of Ω_M and Ω_Λ). This provides a strong, independent cosmological evidence for the existence of dark matter. Figure by Amanullah et al. (2010).

The requirement that dark matter be non-baryonic reduces the range of possible candidates to electrons, neutrinos or a new undiscovered particle. The electron is easily discarded, as any

candidate for dark matter must be "dark" (i.e. it must not emit, reflect or scatter light, since that would be observed) which means that it cannot interact via the electromagnetic force.

Neutrinos are the prototype for what is called "hot" dark matter: They were produced in the Big Bang and their relic abundance today depends on the sum of the flavour masses (Taoso et al., 2008). Hot DM models are out of favour because they tend to to suppress density perturbations below the size scale of superclusters. In other words, they get in the way of galaxy formation. Furthermore, Hot DM predicts a top-down structure formation (i.e. superclusters form first, then clusters, then galaxies) while observations show that structure formation is bottom-up (first galaxies, then larger structures). See (Primack, 2001) for a more complete discussion.

This leaves only two options: Either our theory of gravitation is wrong - an idea first proposed by Milgrom (1983) but with significant problems of its own (e.g. Dodelson, 2011; Chakraborti & Khedekar, 2011) - or dark matter is composed of a new type of undiscovered particle that is stable, neutral, non-baryonic, and much more massive than a neutrino.

1.3 WIMPs

Particle physics provides several candidates to fit the role of dark matter. These are motivated by various unsolved problems in particle physics and they usually go by strange names like Axions, Gravitinos and Sterile neutrinos, or whimsical names like "WIMP" (Weakly Interactive Massive Particles). Of these, WIMPs are the most promising candidates, and this section should give the reader a flavour of why they draw so much interest.

1.3.1 The Higgs mass problem

One of the open problems in particle physics is why the Higgs boson mass appears to be $m_h \sim 100\ \mathrm{GeV/c^2}$, which is much smaller than the Planck mass $M_{Pl} \equiv \sqrt{\hbar c/G} \approx 1.2 \times 10^{19}\ \mathrm{GeV/c^2}$. The mass of the Standard Model Higgs boson is given by $m_h^2 = m_{h0}^2 + \Delta m_h^2$ where m_{h0}^2 and Δm_h^2 are unknown, but Δm_h^2 is a "quantum correction", where

$$\Delta m_h^2 \sim \Lambda^2 \tag{1.1}$$

Λ is the energy scale at which the Standard Model is no longer a valid description of nature. If the Standard Model is correct up to the Planck mass, then $\Lambda \sim M_{Pl}$ and the Higgs mass must be in order of M_{Pl} unless there is a lot of cancellation between m_{h0}^2 and Δm_h^2. In fact:

$$\begin{aligned} \Lambda &\sim M_{Pl} \sim 10^{19}\ \mathrm{GeV/c^2} \\ \Rightarrow \Delta m_h^2 &\sim \Lambda^2 \sim 10^{38}(\ \mathrm{GeV/c^2})^2 \end{aligned}$$

But if this is so, why isn't the Higgs mass $m_h^2 \sim 10^{38}(\ \mathrm{GeV/c^2})^2$ so that $m_h \sim 10^{19}\ \mathrm{GeV/c^2}$? For the Higgs mass to be only $\sim 100\ \mathrm{GeV/c^2}$ requires that m_{h0}^2 also be $\sim 10^{38}(\ \mathrm{GeV/c^2})^2$ in such a way that m_{h0}^2 and Δm_h^2 cancel almost exactly - to 1 part in 10^{36}.

A more plausible alternative is that Λ is in fact much lower. If Λ is in the order of ~ 100 GeV/c^2, it would be more natural that the Higgs mass be ~ 100 GeV/c^2. But this implies that the Standard Model must no longer be valid at ~ 100 GeV/c^2. In other words, there must be new physics (e.g. new particles) in the range of $m \sim 100$ GeV/c^2, which is the range of the weak nuclear force. Other attempts to resolve the Higgs mass problem also lead to new physics at the scale of the weak force. This suggests the existence of a new particle with a mass around the weak scale $m_{weak} \sim 10$ GeV - TeV.

For more information about this, see the excellent review paper by Feng (2010).

1.3.2 Extensions of the standard model

The most natural way to extend the Standard Model is called supersymmetry (Feng, 2010). Supersymmetry assigns to every SM particle a partner that has the same quantum numbers but differs in spin by 1/2. In order words, the supersymmetric partners of matter particles (fermions, with half integer spin) are force-carrying particles (bosons, with full integer spin) and vice versa. For example, the photon is the force carrier of the electromagnetic force. Its supersymmetric partner is the "*photino*", which would be a matter particle. In turn, the sypersymmetric partners of fermions are always spin-zero particles (*scalars*).

The introduction of the new particles supplements the SM quantum corrections Δm_h^2 so that Equation 1.1 becomes:

$$\Delta m_h^2 \sim \left(m_{SUSY}^2 - m_{SM}^2\right) \ln \frac{\Lambda}{m_{SUSY}} \tag{1.2}$$

where m_{SM} and m_{SUSY} are the masses of the SM particles and their superpartners (Feng, 2010). For $m_{SUSY} \sim m_{SM}$, Δm_h is at most $\mathcal{O}(1)$, rescuing the Higgs mass.

What does any of this have to do with dark matter? The plethora of new particles gives several candidates with the right properties to explain dark matter. These particles, collectively known as "*neutralinos*", are the supersymmetric partners of the electroweak bosons and the Higgs boson (for example, the photino a neutralino). These particles all make good dark matter candidates:

- They are all electrically neutral, interacting only by the weak force and gravity. Thus, they do not interact with photons, making them "dark".
- They have a mass around m_{weak}. Thus, they are massive particles, making them good candidates for *cold* dark matter.

Any candidate for dark matter must also be a stable particle, otherwise dark matter would not be present in the modern universe. The lightest neutralino should be a stable particle, making it the primary candidate for dark matter. When one talks about WIMPs, one is normally thinking of the lightest neutralino.

There is another property of neutralinos worth noting: They are all *Majorana* fermions. What that means is that they are their own antiparticle. When two neutralinos meet, they annihilate and convert 100% of their mass into energy. This point will come up again later in this chapter.

1.3.3 The WIMP miracle

The "WIMP miracle" refers to the fact that if a neutralino (a particle motivated by particle physics) indeed exists and is stable, it is naturally produced in the early universe with a relic density consistent with what is required for dark matter (Feng, 2010).

The basic idea is something like this: Take any particle χ that is created in the Big Bang. Initially the universe is hot enough that χ is constantly created and destroyed, so that χ is in thermal equilibrium. At some point the universe cools to a temperature T below the particle mass m_χ, so that χ is no longer created, but it continues to be destroyed via matter - antimatter annihilation. At this point the number of particles drops exponentially as $e^{-m_\chi/T}$. At some later stage, the universe becomes large enough, and the density of χ becomes low enough, that the particles cannot find each other to annihilate. When this happens is a function of the particle speed (which is determined by its mass) and its annihilation cross section. At this point, the particles "freeze out", giving the thermal relic density.

In other words, given a particle's mass and annihilation cross section we can predict its relic density from the Big Bang. Taking a neutralino with mass between 10 GeV and 1 TeV and annihilation cross section consistent with the weak force leads to a relic density that is consistent with what is required for dark matter.

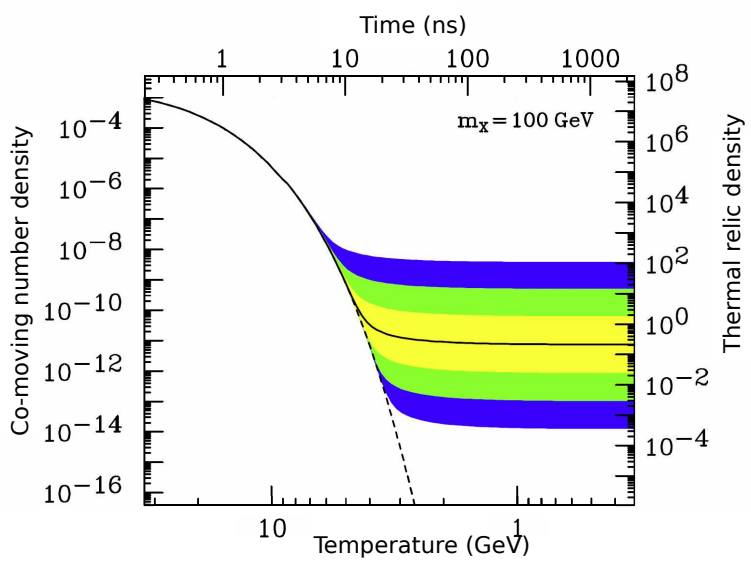

Figure 1.4: The co-moving number density (left) and resulting thermal relic density (right) for a 100 GeV WIMP. The thermal relic density is in units of the critical density, so it represents $\Omega_\chi = \rho_\chi/\rho_{crit}$. The solid contour is for an annihilation cross section that gives the correct relic density. The shaded regions are for cross sections that differ by 10, 100 and 1000 from this value. Figure by Feng (2010).

It is important to note that cosmology places a *lower limit* on the WIMP cross section. Very low cross sections can be discarded because they would make WIMPs over-abundant in the modern universe. This means that sufficiently precise experiments can in principle falsify the WIMP hypothesis. Indeed, Bertone (2010) has suggested that within the next 5 to 10 years WIMPs will be either discovered or discarded as a dark matter candidate.

1.3.4 Summary: WIMPs in three lines

For the purposes of this work, there are three key pertinent facts about WIMPs:

1. WIMPs are massive particles. At $m_X \sim 100$ GeV/c^2, they are about 100 proton masses.
2. WIMPs interact only by the weak nuclear force and gravity.
3. WIMPs are their own antiparticle. When two WIMPs meet, they annihilate.

1.4 Experiment and detection of dark matter

Via the weak interaction, WIMPs can collide with Standard Model particles and scatter. Most detection experiments try to detect this scatter directly, in a manner reminiscent of neutrino experiments. There are several ways that a neutralino could interact with a Standard Model particle via the weak force; some couplings require particle spin while others do not. Thus, the WIMP-nucleon interaction has a spin-dependent and a spin-independent cross section (σ_{SD} and σ_{SI}). This section describes some of the key experiments that constraint $\sigma_{SD,SI}$ and may one day detect WIMPs.

1.4.1 Direct detection experiments

Direct detection experiments such as XENON10 (Angle et al., 2008), ZEPLIN III (Lebedenko et al., 2009), EDELWEISS II (Armengaud et al., 2010), CDMS II (CDMS II Collaboration et al., 2010) and DAMA (Bernabei et al., 2008) try to detect collisions with a material in the lab. These normally probe the spin-independent cross section, since most most materials available on Earth are made of atoms with an even number of nucleons, and hence have no net spin. Figure 1.5 shows the limits imposed by XENON10, ZEPPLIN III, EDELWEISS II and CDMS II. Observe that these experiments exclude some of the parameter space predicted by supersymmetric models, but the bulk of the parameter space remains unexplored.

In recent years the DAMA project has detected an annual modulation signature for dark matter particles (Bernabei et al., 2008). This result remains unconfirmed by other experiments. Figure 1.5 shows the 3 σ favoured region from the DAMA signal. The DAMA results could be made compatible with other experiments if we postulate dark matter particles with lower mass ($m_X \sim 10$ GeV/c^2) and larger cross section ($\sigma_{SI} \sim 10^{-43}$ cm^2) than expected for neutralinos. However, in this thesis I take the more traditional values of $m_X = 100$ GeV/c^2 and $\sigma_{SI} = 10^{-44}$ cm^2.

1.4.2 Indirect detection experiments

There are several indirect detection methods being pursued. Perhaps the most important is the study of solar neutrinos, which is an indirect way to probe the spin-dependent scatter cross section (see below). Therefore, this method complements and competes with the direct search experiments discussed earlier.

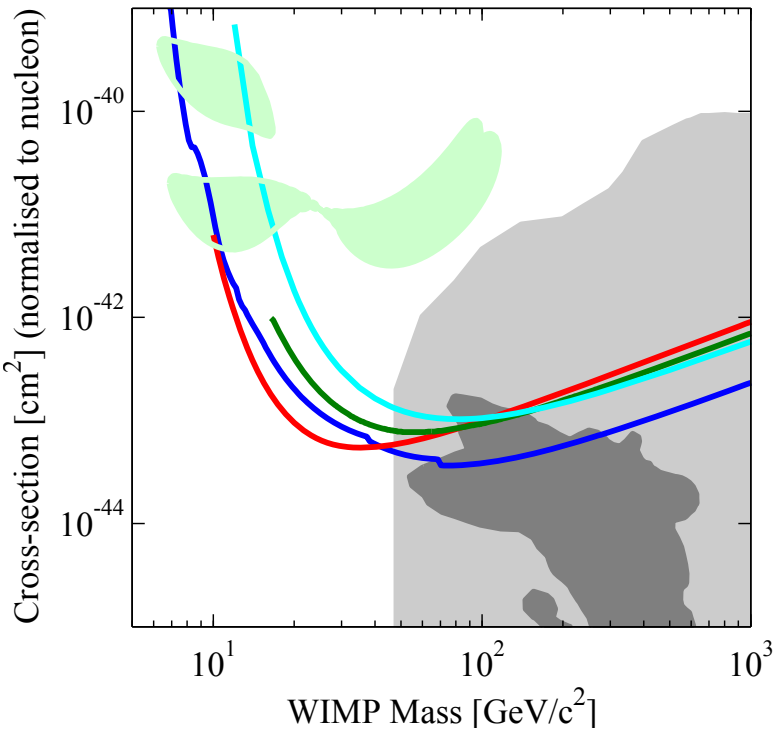

Figure 1.5: Upper bounds on spin-independent WIMP-nucleon cross sections σ_{SI} from XENON10 (red), ZEPLIN III (green), EDELWEISS II (light blue), and CDMS II (blue), along with the combined 3 σ favoured regions (green shaded) from DAMA. The lower right shaded regions are predictions for neutralino dark matter in the general minimal supersymmetric standard model (Kim et al., 2002) (light grey) and minimal supergravity (Trotta et al., 2008) (dark grey). Figure by Feng (2010).

How the Sun captures WIMPs

The basic idea is that WIMPs going through the Sun can collide with nuclei in the Sun (mainly hydrogen) and slow down. Some WIMPs will be slowed down below escape velocity so they become captured by the Sun. Once captured, additional collisions reduce the size of the WIMP orbit until the WIMP settles at the centre of the Sun. Therefore, at the centre of the Sun there ought to be a high density of WIMPs, so that they can more easily collide with each other and annihilate (Feng, 2010).

The capture of WIMPs by a star is completely dominated by hydrogen. The main reason for this is not that hydrogen is more abundant, but that a hydrogen nucleus has a net spin, so it participates in the spin-dependent weak interaction. As we shall see later, the spin-dependent interaction has a much larger cross section. For this reason, detection methods that are based on WIMP capture by stars effectively probe the spin-dependent cross section.

From WIMPs to solar neutrinos

Although most of the products of WIMP annihilation are immediately absorbed, neutrinos are not. Neutrinos produced by WIMP annihilation exit the Sun and can be detected on Earth by neutrino experiments. The total flux of neutrinos depends on the WIMP density, which results

from the competing processes of WIMP capture and WIMP annihilation. A large body like the Sun has reached equilibrium so that *Capture rate* $= 2 \times$ *Annihilation rate* (Feng, 2010).

The capture rate is determined by the spin-dependent cross section, however, this is not enough to completely determine the neutrino flux. It is necessary to make some assumptions about how neutrinos are produced (Feng, 2010). This makes solar neutrinos an imperfect way to probe the spin-dependent cross section. Figure 1.6 shows the upper bounds for spin-dependent WIMP cross sections σ_{SD} from various experiments. The shaded region is a prediction for neutralinos in the general minimal supersymmetric standard model under certain assumptions (For details, see Feng, 2010).

Notice in Figure 1.6, that the spin-dependent cross section σ_{SD} is $\sim 10^4$ times larger than the spin-independent cross section σ_{SI}. This is the reason why WIMP capture inside a star is dominated by hydrogen (which has spin). Notice also that the spin-dependent cross section is much less constrained. The solar neutrino experiments are only starting to scratch the surface of the parameter space, while the direct detection experiments have already excluded large regions (Figure 1.5).

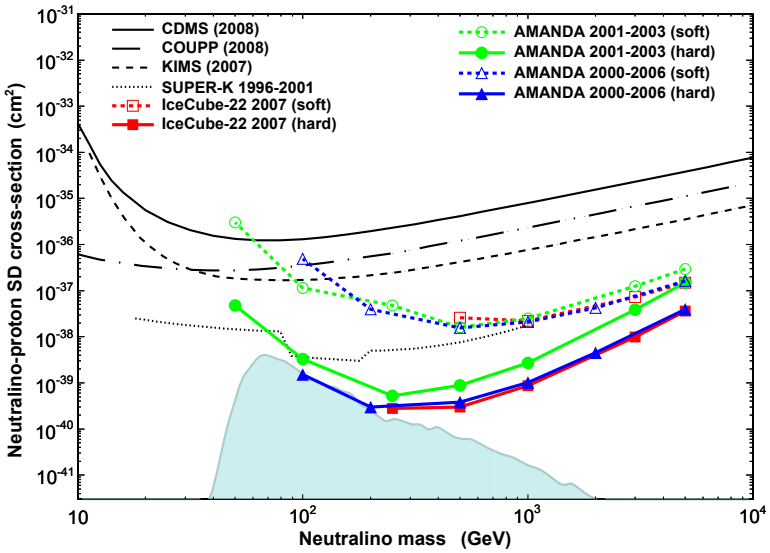

Figure 1.6: Upper bounds on spin-dependent cross sections σ_{SD} from CDMS (Ahmed et al., 2009), COUPP (Behnke et al., 2008), KIMS (Lee et al., 2007), Super-K (Desai et al., 2004), and IceCube (Abbasi et al., 2009). The shaded region is a prediction for neutralinos in the general MSSM under certain assumptions (Ref, Braun et al., 2009). Figure from Feng (2010) with modifications.

1.4.3 Direct production at the LHC

There is also the tantalizing possibility that dark matter particles (WIMP or otherwise) might be produced directly by the Large Hadron Collider. Even if these particles are not produced directly, knowing the Higgs mass would constrain supersymmetric models.

Indeed, the ATLAS and CMS collaborations have reported signals that suggest a Higgs mass around 125 GeV, and Moroi & Nakayama (2011) has suggested that this fits most naturally with supersymmetric models where the Wino (the supersymmetric partner of the W^+ and W^- bosons) is the lightest superparticle and has a mass of a few hundred GeV.

1.4.4 Limits used in this thesis

In light of existing limits on WIMP mass and cross section (Figures 1.5 and 1.6), this thesis uses the following WIMP parameters:

$$\begin{aligned} m_X &= 100 \text{ GeV} / \text{c}^2 \\ \sigma_{SI} &= 10^{-44} \text{ cm}^2 \\ \sigma_{SD} &= 10^{-38} \text{ cm}^2 \end{aligned}$$

According to Figure 1.6, a value of $\sigma_{SD} = 10^{-39}$ cm^2 might be more appropriate, but part of the purpose of this thesis is to compare results with previous research such as the work of Scott et al. (2009), which uses $\sigma_{SD} = 10^{-38}$ cm^2.

1.5 WIMPs and stars

1.5.1 Possible observables

Section 1.4.2 explained how WIMP particles are captured by the Sun. Once WIMPs are captured, they will drop to lower orbits until they reach thermal equilibrium. The temperature at the centre of the Sun is $\sim 1.5 \times 10^7$ K, which for a 100 GeV particle gives a typical speed of:

$$v = \sqrt{\frac{3\,k\,T}{m_X}} = 59 \text{ km s}^{-1}$$

This corresponds to an orbit well inside the Sun's core. The consequences of this were first explored in the 1980s, as a possible way to solve the solar neutrino problem at the time. The basic idea is that WIMPs concentrated at the core can be very efficient at transporting heat out of the hot, neutrino-producing core. Thus, they would lower the core temperature and the neutrino signature (See Spergel & Press, 1985; Press & Spergel, 1985; Krauss et al., 1985).

The discovery of neutrino oscillations has since resolved the solar neutrino problem. However, the idea of WIMP-driven heat transport was revived recently by Hamerly & Kosovichev (2011), who proposed that the change in temperature could be detected via Helioseismology. In brief, the change in the Sun's temperature profile would alter the propagation of sound waves through the Sun, and this could be detected (Hamerly & Kosovichev, 2011). One attractive aspect of this proposal is that it does not require WIMPs to annihilate, so it may be suitable for a broader class of dark matter candidates.

In the context of traditional neutralino dark matter, self-annihilation provides another mechanism through which WIMPs could affect stars: As WIMPs annihilate at the centre of a star, they convert their mass into energy. The exact decay mechanism depends on the precise particle model, but in general one can expect that a fraction of the energy will escape in the form of

neutrinos and a fraction stays in the star. Thanks to the significant energy released by matter-antimatter annihilation, even a small mass of captured WIMPs could add significant energy to a star and change its evolution. The most obvious effect is that a star would not need to burn as much hydrogen to hold itself up against gravity. Additionally, increasing the temperature gradient at the centre of the star can cause the star's core to become convective. In a typical star, only the hydrogen in the core ever undergoes fusion. A convective core would allow the core to mix with the star's envelope, constantly replenishing the hydrogen at the core. This would dramatically increase the lifetime of a star (Scott et al., 2009).

1.5.2 Capture rate

Can stars capture enough WIMPs to change their interior or alter their evolution? The WIMP capture rate depends on the local WIMP density and the speed at which WIMPs cross the star. Slower moving WIMPs have less total energy and hence are easier to capture.

Since WIMPs behave as collision-less particles, they should form a spherical halo in which the Galaxy sits. Computer simulations have been used for some time to determine the density profile of the dark matter halo (Navarro et al., 1996; Moore et al., 1999; Navarro et al., 2004; Diemand et al., 2007). Halos are typically modelled as a quasi-power law with $\rho_\chi \propto r^\gamma$ where γ is more negative in the outer parts of the halo than in the inner region. In addition, the high density of baryonic matter in the galactic centre may be expected to produce a sharp spike near the centre (Gustafsson et al., 2006).

The velocity distribution is more straight forward: the WIMP halo has a Maxwellian (i.e. isothermal) speed distribution:

$$f_0(v) = \frac{4}{\sqrt{\pi}} \left(\frac{3}{2}\right)^{3/2} \frac{v^2}{\overline{v}^3} \exp\left(\frac{-3\,v^2}{2\,\overline{v}^2}\right) \tag{1.3}$$

Where v is the WIMP speed (before it is affected by the star's gravity) and $\overline{v}$ is the velocity dispersion, which is determined by the galactic potential. In the reference frame of a star moving with speed of $v_\star$, the speed distribution becomes:

$$f_\star(v) = f_0(v)\ \exp\left(\frac{-3\,v_\star^2}{2\,\overline{v}^2}\right) \frac{\sinh(3\,v\,v_\star/\overline{v}^2)}{3\,v\,v_\star/\overline{v}^2} \tag{1.4}$$

1.5.3 How to enhance WIMP capture

A star can typically only capture the small fraction of WIMPs moving with very low relative velocities. Slower WIMPs have less energy, so they do not need to lose as much energy to be captured. Equation 1.4 shows that the WIMP speed distribution is determined by the star's own speed in the galactic frame. Intuitively, the faster a star moves around the galaxy, the faster the WIMP halo appears to move from the star's reference frame.

This observation led Scott et al. (2009) to consider stars with very eccentric orbits, very near the galactic centre. The idea is that at the galactic centre the WIMP density is high, and the highly eccentric orbit allows the star to have a low relative speed. Scott et al. (2009) found that for a very tight, 10-year orbit around the galactic centre, an eccentricity of $e \approx 0.99$ boosted the mean capture rate by up to 20 orders of magnitude compared to a circular orbit.

1.5.4 Binary stars and capture rate

In this thesis I explore a alternative way to change a star's speed in the galactic frame: If a star is in a binary, its speed relative to the galaxy and the WIMP halo constantly changes. The basic idea is that during part of its orbit the star moves slowly and can capture many more WIMPs, so that after a complete orbit, the binary might boost WIMP capture.

For this project, it will be necessary to do a detailed N-body simulation that correctly models the passage and capture of WIMPs in a binary system. The gravitational interaction between the WIMP and the two stars might play an important role, as close encounters either eject WIMPs, or scatter them into bound orbits. When the N-body simulation code is complete, it will be important to consider different types of binaries. An obvious candidate is close binaries where the binary orbital speed is comparable to the speed of stars around the galaxy.

A similar idea was recently explored by Brayeur & Tinyakov (2011), in a short paper that studied dark matter capture by neutron stars in close binaries. In this paper they propose that dark matter accumulation by compact stars may eventually lead to a collapse into a black hole. The work in this thesis differs from the work of Brayeur & Tinyakov (2011) in that I am considering main sequence stars, where a small mass of captured WIMPs could visibly alter the star's evolution through matter-antimatter annihilation.

Chapter 2

WIMP-nucleus collision model

2.1 Speed of WIMPs and stellar nuclei

2.1.1 Speed of nuclei inside the star

Figure 2.1 shows the average speed of atomic elements at the range of temperatures found inside a star. This is simply a plot of Equation 2.1

$$\frac{1}{2}mv^2 = \langle E \rangle = \frac{3}{2}kT \quad \Rightarrow \quad v = \sqrt{\frac{3kT}{m}} \tag{2.1}$$

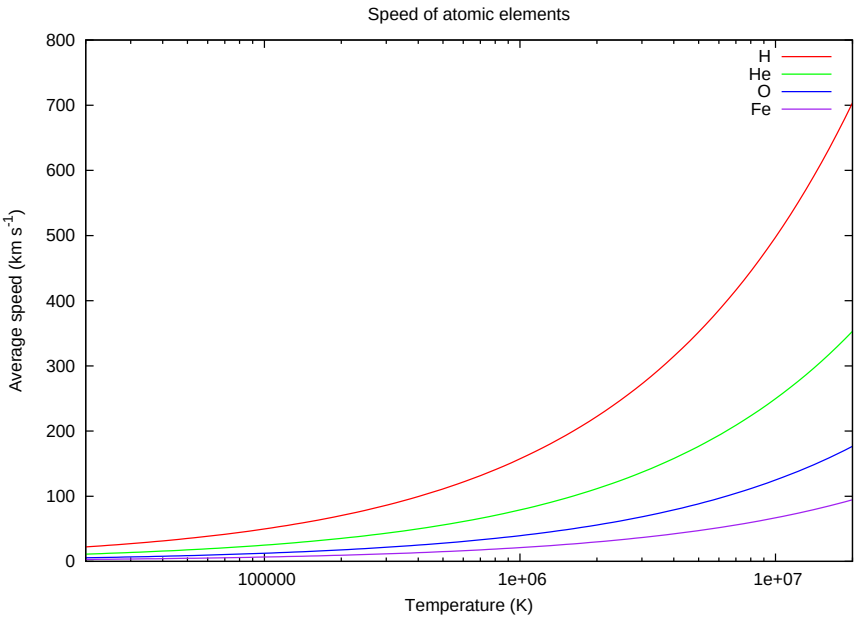

Figure 2.1: Average speeds of atomic nuclei for the temperatures typically found inside a star. The Sun's photosphere has a temperature between 5700 K and 8900 K, while the temperature inside the Sun's core reaches 1.57×10^7 K.

2.1.2 Speed of capturable WIMPs

Most WIMPs travel too fast to be captured by a star. A good first step is to determine the range of WIMP speeds that are slow enough to permit capture after a collision with stellar material. Let v_∞ be the WIMP speed away from the star's gravitational influence. Scott et al. (2009) gives the maximum speed at which a WIMP can be captured:

$$v_\infty \leq \frac{2v_e\sqrt{m_\chi m_N}}{m_\chi + m_N}$$

Where v_e is the local escape velocity. Let v_χ be the speed of the WIMP inside the star. Then $v_\chi^2 = v_\infty^2 + v_e^2$ and using the above relation one obtains:

$$v_\chi \leq \left(\frac{m_\chi + m_N}{m_\chi - m_N}\right) v_e \tag{2.2}$$

Table 2.1 shows the maximum capturable speed for various elements, assuming a WIMP mass of 100 GeV. For reference, the Sun's escape velocity at the surface is about $600\,km\,s^{-1}$.

Table 2.1: Most accurate data sets

	H	He	O	Fe
$v_\chi \leq$	$1.02\,v_e$	$1.08\,v_e$	$1.35\,v_e$	$3.17\,v_e$

2.1.3 Capture in the context of a binary system

In a binary system, a WIMP that has a speed less than the escape velocity of a star, will not necessarily remain bound to that star. The gravity of the companion star might cause the WIMP to be trapped by the companion, or even to get ejected from the system entirely.

At which point can one be certain that a WIMP cannot be lost due to the companion's gravity? One reasonable choice is to declare a WIMP captured when it no longer has enough energy to leave the star's Roche lobe.

Given two stars M_1, M_2 with separation a, the Roche lobe radius of M_1 is approximately:

$$\frac{r_l}{a} = 0.462\left(\frac{M_1}{M_1 + M_2}\right)^{1/3}$$

The requirement that the WIMP never leave the Roche lobe can be expressed as an upper bound on the WIMP velocity:

$$v \leq \sqrt{v_e^2 - \frac{2GM}{r_l}}$$

Where v_e is the local escape velocity.

2.2 Mechanics of collision

2.2.1 Velocity of the centre of mass

In a two-particle system the total momentum is $\boldsymbol{p}_{tot} = m_1\boldsymbol{v}_1 + m_2\boldsymbol{v}_2$. By definition, the velocity of the centre of mass $\boldsymbol{v}_{\text{com}}$ is the velocity such that $\boldsymbol{p}_{tot} = (m_1 + m_2)\boldsymbol{v}_{\text{com}}$. Thus, in a collision between a WIMP and an atomic nucleus, the centre of mass velocity is:

$$\boldsymbol{v}_{\text{com}} = \frac{m_\chi \boldsymbol{v}_\chi + m_N \boldsymbol{v}_N}{m_\chi + m_N} \tag{2.3}$$

Considering the significant mass of the WIMP compared to most atomic nuclei, it is tempting to assume $m_\chi \boldsymbol{v}_\chi \gg m_N \boldsymbol{v}_N$ and approximate the above equation as $\boldsymbol{v}_{\text{com}} \approx \frac{m_\chi \boldsymbol{v}_\chi}{m_\chi + m_N}$. This is a good approximation provided that the speed of the WIMP is not lower than the speed of nuclei in the star, but it may not be applicable to WIMPs that have already been captured. Thus, I shall not use this approximation.

2.2.2 WIMP velocity after a collision

In this section I use Equation 2.3 to derive the velocity of a WIMP particle after a collision with an atomic nucleus inside a star. For this derivation it is first necessary to define a few symbols:

$$\begin{aligned}
\boldsymbol{v}_{\text{com}} &\equiv \text{Velocity of the WIMP-nucleus centre of mass.} \\
\boldsymbol{v}_\chi, \boldsymbol{v}_N &\equiv \text{Velocity of the WIMP and nucleus in the star's frame.} \\
\boldsymbol{u}_\chi, \boldsymbol{u}_N &\equiv \text{Velocity of the WIMP and nucleus in the centre of mass frame.} \\
&\quad \text{For example } \boldsymbol{u}_\chi = \boldsymbol{v}_\chi - \boldsymbol{v}_{\text{com}} \\
\hat{\boldsymbol{i}}, \hat{\boldsymbol{j}} &\equiv \text{Orthonormal vectors with } \hat{\boldsymbol{i}} = \hat{\boldsymbol{u}_\chi} \text{ and } \hat{\boldsymbol{j}} \text{ orthogonal to } \hat{\boldsymbol{i}}. \\
u &\equiv \|\boldsymbol{u}_\chi\| \qquad v_\chi \equiv \|\boldsymbol{v}_\chi\| \qquad v_N \equiv \|\boldsymbol{v}_N\| \\
\mu_\chi &\equiv \frac{m_\chi}{m_\chi + m_N} \qquad \mu_N \equiv \frac{m_N}{m_\chi + m_N}
\end{aligned}$$

The formula for the centre of mass can be rewritten as: $\boldsymbol{v}_{\text{com}} = \mu_\chi \boldsymbol{v}_\chi + \mu_N \boldsymbol{v}_N$. The velocity $\boldsymbol{v}_N$ can be decomposed in terms of $\hat{\boldsymbol{i}}$ and $\hat{\boldsymbol{j}}$ as:

$$\boldsymbol{v}_N = v_N(\hat{\boldsymbol{i}} \cos\alpha + \hat{\boldsymbol{j}} \sin\alpha) \tag{2.4}$$

In Equation 2.4, α is the angle between $\boldsymbol{v}$ and $\boldsymbol{u}_\chi = \boldsymbol{v}_\chi - \boldsymbol{v}_{\text{com}}$. This decomposition may not be intuitive, but I have chosen it because it makes it easier to relate the velocities in the star frame ($\boldsymbol{v}_N$ and $\boldsymbol{v}_\chi$) with those in the centre-of-mass frame ($\boldsymbol{u}_N$ and $\boldsymbol{u}_\chi$). This decomposition is illustrated in Figure 2.2.

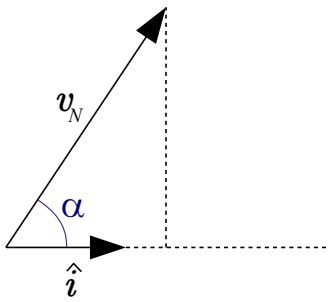

Figure 2.2: The velocity of a nucleus in the star's frame $\boldsymbol{v}_N$ can be written in terms of $\hat{\boldsymbol{i}}$, which is the unit vector parallel to $\boldsymbol{u}_\chi = \boldsymbol{v}_\chi - \boldsymbol{v}_{\rm com}$. This decomposition makes it easier to relate the velocities in the star frame ($\boldsymbol{v}_N$ and $\boldsymbol{v}_\chi$) with those in the centre-of-mass frame ($\boldsymbol{u}_N$ and $\boldsymbol{u}_\chi$).

Using Equation 2.4 together with $\boldsymbol{u}_\chi = \boldsymbol{v}_\chi - \boldsymbol{v}_{\rm com}$ we can derive a corresponding formula for $\boldsymbol{v}_\chi$ in terms of α:

$$\begin{aligned}
\boldsymbol{u}_\chi &= \boldsymbol{v}_\chi - \boldsymbol{v}_{\rm com} = u\,\hat{\boldsymbol{i}} \\
&\Rightarrow\ u\,\hat{\boldsymbol{i}} = \boldsymbol{v}_\chi - \mu_\chi \boldsymbol{v}_\chi - \mu_N \boldsymbol{v}_N \\
&\Rightarrow\ u\,\hat{\boldsymbol{i}} = (1-\mu_\chi)\boldsymbol{v}_\chi - \mu_N \boldsymbol{v}_N \\
&\Rightarrow\ (1-\mu_\chi)\boldsymbol{v}_\chi = u\,\hat{\boldsymbol{i}} + \mu_N \boldsymbol{v}_N \\
&\Rightarrow\ \mu_N \boldsymbol{v}_\chi = u\,\hat{\boldsymbol{i}} + \mu_N v_N(\cos\alpha\hat{\boldsymbol{i}} + \sin\alpha\hat{\boldsymbol{j}}) \\
&\therefore\ \boldsymbol{v}_\chi = (\frac{u}{\mu_N} + v_N\,\cos\alpha)\hat{\boldsymbol{i}} + (v_N\,\sin\alpha)\hat{\boldsymbol{j}}
\end{aligned}$$

Putting this back into the formula for $\boldsymbol{v}_{\rm com}$ gives:

$$\therefore \boldsymbol{v}_{\rm com} = (\frac{u\,\mu_\chi}{\mu_N} + v_N\,\cos\alpha)\hat{\boldsymbol{i}} + (v_N\,\sin\alpha)\hat{\boldsymbol{j}}$$

Now it is possible to calculate the WIMP velocity $\boldsymbol{v}'_\chi$ after the collision. Let θ be the scatter angle in the centre of mass frame (Figure 2.3). Using the fact that in the centre of mass frame $\|\boldsymbol{u}\| = \|\boldsymbol{u}'\| = u$, we can write the post-collision speed as:

$$\boldsymbol{u}'_\chi = u\,\cos\theta\,\hat{\boldsymbol{i}} + u\,\sin\theta\,\hat{\boldsymbol{j}}$$

In the star frame this becomes:

$$\boldsymbol{v}'_\chi = u\,\cos\theta\,\hat{\boldsymbol{i}} + u\,\sin\theta\,\hat{\boldsymbol{j}} + \boldsymbol{v}_{\rm com}$$

Which then simplifies to:

$$\therefore \boldsymbol{v}'_\chi = \left[u\left(\frac{\mu_\chi}{\mu_N} + \cos\theta\right) + v_N\cos\alpha\right]\hat{\boldsymbol{i}} + \left[u\sin\theta + v_N\sin\alpha\right]\hat{\boldsymbol{j}}$$

Using $\mu_\chi/\mu_N = m_\chi/m_N$ this formula becomes:

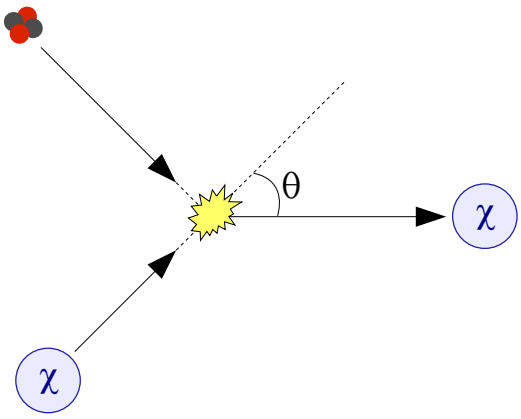

Figure 2.3: Deflection angle θ in the centre of mass frame.

$$\therefore \boldsymbol{v}'_\chi = \left[u\left(\frac{m_\chi}{m_N} + \cos\theta\right) + v_N \cos\alpha\right]\hat{\boldsymbol{i}} + \left[u\sin\theta + v_N \sin\alpha\right]\hat{\boldsymbol{j}} \tag{2.5}$$

The final step is to calculate u. This value can be obtained from the formula for $\boldsymbol{v}_\chi$:

$$v_\chi^2 = (\frac{u}{\mu_N} + v_N\ \cos\alpha)^2 + (v_N\ \sin\alpha)^2$$

$$\therefore u = \mu_N\left(\sqrt{v_\chi^2 - v_N^2\ \sin^2\alpha}\right) - \mu_N\, v_N\ \cos\alpha \tag{2.6}$$

2.2.3 Energy loss after a collision

It is most convenient to express the energy loss as a fractional value:

$$\Delta \equiv \frac{\Delta E}{E} = \frac{v_\chi^2 - v_\chi'^2}{v_\chi^2} \tag{2.7}$$

Figures 2.4 and 2.5 illustrate how Δ changes with the scatter angle θ and with the WIMP's position inside the star. These figures merit some explanation:

- The figures model a 100 GeV WIMP travelling at escape velocity through the Sun.
- For any given radius and scatter angle θ, there is a range of possible exit velocities (and energies) depending on the angle at which the WIMP collides with the atomic nucleus. This is the angle α in Equations 2.5 and 2.6. This is the reason why Figures 2.4 and 2.5 show thick bands rather than just a thin line.
- Figure 2.4 plots Δ vs θ for $r = R_\odot/2$, while Figure 2.5 plots Δ vs r for $\theta = \pi$.

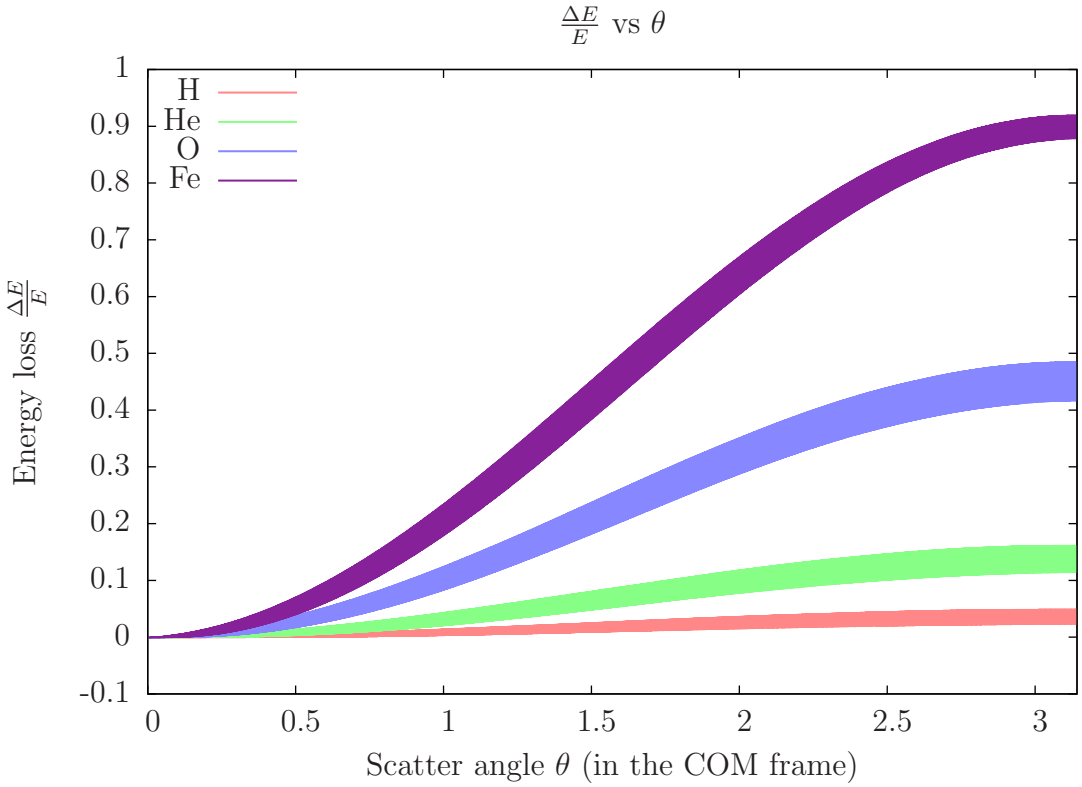

Figure 2.4: Fraction of kinetic energy lost by a 100 GeV WIMP colliding with an atomic nucleus inside the Sun as a function of the WIMP scatter angle in the centre of mass frame. The collision occurs at a distance $r = R_\odot/2$ from the core and the WIMP travels at escape velocity. The spread (thickness) of the bands covers the possible range of collision angles between the WIMP and the atomic nucleus. See Figure 2.5 for a complementary picture of WIMP-nucleus collisions.

2.3 Probability distributions

To model WIMP scatter inside the Sun requires two probability distributions:

- What is the probability that a collision occurs?
- Given a collision, what is the probability distribution of the exit angle θ?

These probabilities are both determined by the WIMP-nucleus interaction cross section.

2.3.1 Interaction cross section

For the purpose of detection, the most important property of a WIMP is its interaction cross section with ordinary matter. This cross section determines the likelihood of detection in direct-detection experiments, and it determines the rate at which particles from the WIMP halo are captured by the Sun or any star.

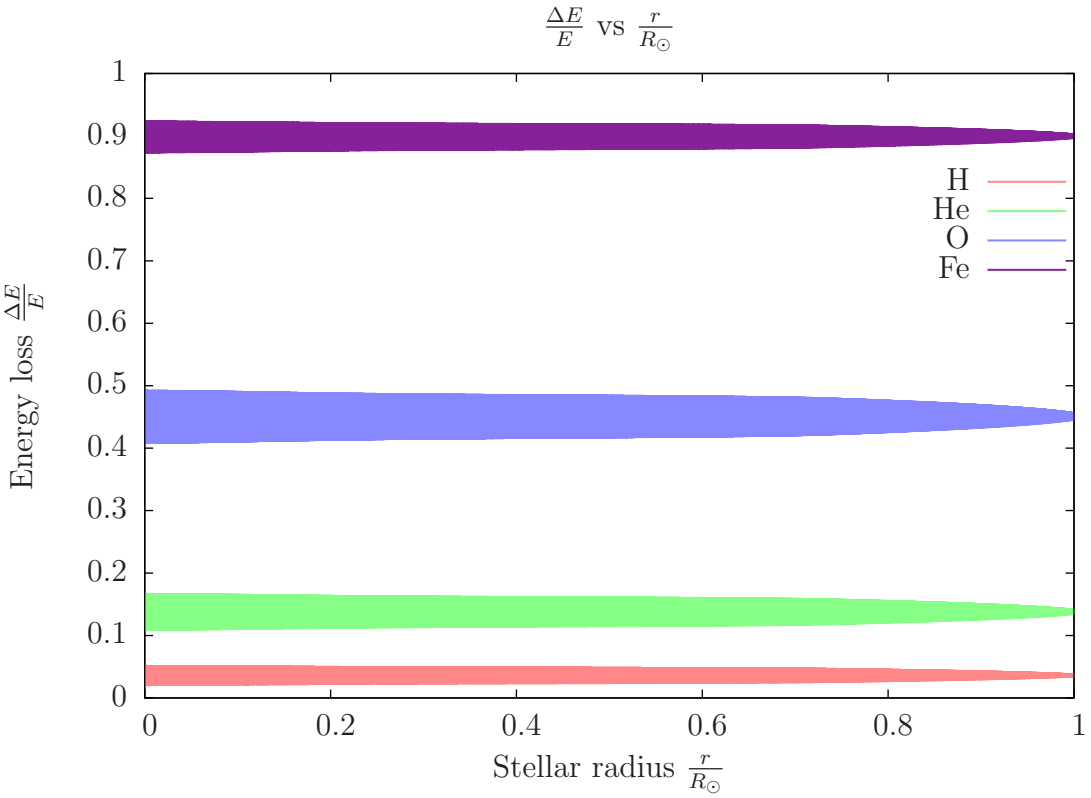

Figure 2.5: Fraction of kinetic energy lost by a 100 GeV WIMP colliding with an atomic nucleus inside the Sun as a function of the location inside the Sun where the collision occurs. In all cases the WIMP travels at escape velocity and the WIMP scatter angle in the centre of mass frame is $\theta = \pi$. The spread (thickness) of the bands covers the possible range of collision angles between the WIMP and the atomic nucleus. See Figure 2.4 for a complementary picture of WIMP-nucleus collisions.

There is good reason to believe that WIMPs have a finite (i.e. non-zero) interaction cross section. If they did not, they would not have annihilated in the early universe and WIMPs would be unacceptably over-abundant today (Jungman et al., 1996). A fully accurate calculation of the WIMP-nucleus cross section requires detailed nuclear calculations (e.g. Ressell et al., 1993). However, a simple nuclear model can provide reasonable estimates which are more than sufficient given the factor-of-two uncertainties in the local halo density and velocity dispersion of the various WIMP models (Jungman et al., 1996, pp. 295).

As shown by Jungman et al. (1996), a WIMP generally scatters from nuclei with spin, (which for the purpose of capture by a star only includes hydrogen) via spin-dependent interaction. Furthermore, the spin-dependent cross section is uniform. In contrast, if the neutralino scatters via spin-independent interaction, then at high momentum transfer there will be a form-factor suppression to the cross section. If the momentum transfer $\boldsymbol{q}$ is not small compared to the inverse of the nuclear radius R, the neutralino does not "see" the entire nucleus. In brief:

	Interaction	Cross section
Hydrogen	Spin-dependent	$\sigma = \sigma_{SD}$ (constant)
Other elements	Spin-independent	$\sigma = \sigma_0 \cdot F(\boldsymbol{q})$

Where $F(\boldsymbol{q})$ is the form-factor. The form factor and σ_0 both depend on the nuclear species. Scott et al. (2009) approximate σ_0 as:

$$\sigma_0 = \sigma_{SI} \left(\frac{m_N(m_\chi + m_H)}{m_H(m_\chi + m_N)} \mathcal{A} \right)^2 \tag{2.8}$$

Where m_H is the mass of hydrogen and $\mathcal{A}$ is the atomic number of the nucleus. Constraints on σ_{SI} and σ_{SD} were discussed in section 1.4. As mentioned in section 1.4.4, this thesis will use:

$$\begin{aligned} \sigma_{SI} &= 10^{-44}\ \mathrm{cm}^2 \\ \sigma_{SD} &= 10^{-38}\ \mathrm{cm}^2 \end{aligned}$$

Table 2.2: Cross sections for common elements

	Cross section (cm^2)
^{1}H	$\sim 10^{-38}$
^{4}He	$\sim 10^{-42} \cdot F(\boldsymbol{q})$
^{8}O	$\sim 10^{-40} \cdot F(\boldsymbol{q})$
^{26}Fe	$\sim 10^{-38} \cdot F(\boldsymbol{q})$

Table 2.2 gives the cross section for some common elements. For an isotropic cross section, the form factor can be written in terms of the energy transfer Δ, which Scott et al. (2009) approximates as:

$$F(\Delta) = \exp\left(-\frac{E_\chi}{E_0}\Delta\right) \tag{2.9a}$$

$$E_0 \approx \frac{5.8407 \times 10^{-2}}{m_N \left(0.91 m_N^{1/3} + 0.3\right)^2}\mathrm{GeV} \qquad E_\chi \equiv \frac{1}{2} m_\chi v_\chi^2 \tag{2.9b}$$

Where m_N is expressed in GeV/c^2. An exponential form factor is a good approximation for the case of spin-independent interaction (Jungman et al., 1996). For light elements such as helium, $F(\Delta) \approx 1$ and the cross section is essentially constant. For oxygen, $F(\Delta)$ can reduce σ by as much as a factor of 2, and for iron, $F(\Delta)$ can reduce σ by as much as two orders of magnitude. Recall that for Hydrogen, the neutralino scatters via spin-dependent interaction and suffers no form factor suppression.

2.3.2 Probability of collision

Let n_k be the number density of the k^{th} nuclear species in the star, and let v be the speed of the WIMP inside the star. Let $s(t)$ be the path of a WIMP through the Sun in the absence of collisions. The probability of scatter in a small path element δs is:

$$P_{col}(s)\delta s = \left(1 - \int_{s_0}^{s} P(s')ds'\right) \sum_k \langle \sigma_k(s) \rangle \, n_k(s) \, \delta s \tag{2.10}$$

Where $\langle \sigma \rangle$ is the mean cross section. The integral reflects the fact that the probabilities are not independent (if the WIMP collides at one point s_1, it will follow a new trajectory from that point on). However, if a WIMP has a low probability of collision ($\int P_{col}(s')ds' \ll 1$), this equation can be simplified to:

$$P_{col}(r) \, \delta r \approx \sum_k \langle \sigma_k(r) \rangle \, n_k(r) \, \delta r \tag{2.11}$$

Notice that the equation has been rewritten in terms of the radial distance r. This is the formula that will be used in this thesis. The mean cross section $\langle \sigma \rangle$ can be obtained by averaging over all possible scatter angles θ. In other words:

$$\begin{aligned} \langle \sigma \rangle &= \frac{\int \sigma(\theta) \times (\text{Surface of the ring at angle } \theta)}{\text{Surface of a sphere}} \\ &= \frac{\int \sigma(\theta) \times (2\pi \cdot r \sin\theta \cdot r d\theta)}{4\pi r^2} \\ &= \frac{1}{2} \int \sigma(\theta) \cdot \sin\theta \, d\theta \end{aligned}$$

For Hydrogen this gives $\langle \sigma \rangle = \sigma_{SD}$ and for other elements $\langle \sigma \rangle = \sigma_0 \frac{1}{2} \int F(\Delta) \cdot \sin\theta \, d\theta$

2.3.3 Probability of angle θ

Let P_θ be the probability distribution of the exit angle θ once a collision has occurred. By a similar argument to the previous section, this probability distribution is:

$$P_\theta(\theta) = \frac{\frac{1}{2}\sigma(\theta)\sin\theta}{\frac{1}{2}\int \sigma(\theta')\sin\theta' d\theta'}$$

For Hydrogen this simply becomes $P_\theta = \frac{1}{2}\sin\theta$. For other elements, the formula simplifies to:

$$P_\theta(\theta) = \frac{F(\Delta)\sin\theta}{\int F(\Delta')\sin\theta' d\theta'} \tag{2.12}$$

For any element where $F(\Delta)$ is approximately independent of θ, this becomes $P_\theta \approx \frac{1}{2}\sin\theta$.

2.4 Approximation and final model

For the purpose of simulating the capture of WIMPs by a star, the most important quantities are the form factor (Equation 2.9) as that gives the probability of interaction, and the velocity of the WIMP after a collision $\boldsymbol{v}'_\chi$ (Equation 2.5). The simplest approximation is to set $\alpha = 0$ in Equations 2.5 and 2.6. Of the most common elements in the Sun, iron has the largest atomic mass, and therefore, the largest form factor suppression (Equation 2.9). If the approximation $\alpha = 0$ is sensible for iron, it will be sensible for other elements. Figure 2.6 shows the form factor of iron as a function of position inside the star. The figure shows three curves:

- $F(\Delta)$ if $\alpha \equiv 0$.
- $F(\Delta)$ if $\alpha \equiv \pi$.
- The mean value of $F(\Delta)$, averaged over all angles $\alpha \in (0, 2\pi)$.

The figure shows that the approximation $\alpha \equiv 0$ gives roughly the correct form factor suppression throughout the star. In fact, in the worst case scenario (a WIMP colliding with iron at the centre of the Sun), the error in the form factor is only $\sim 17\%$. As will be shown later, WIMP capture is completely dominated first by hydrogen, and second by lighter elements such as helium and oxygen, a $\lesssim 17\%$ error for iron will have no effect on the results of this project.

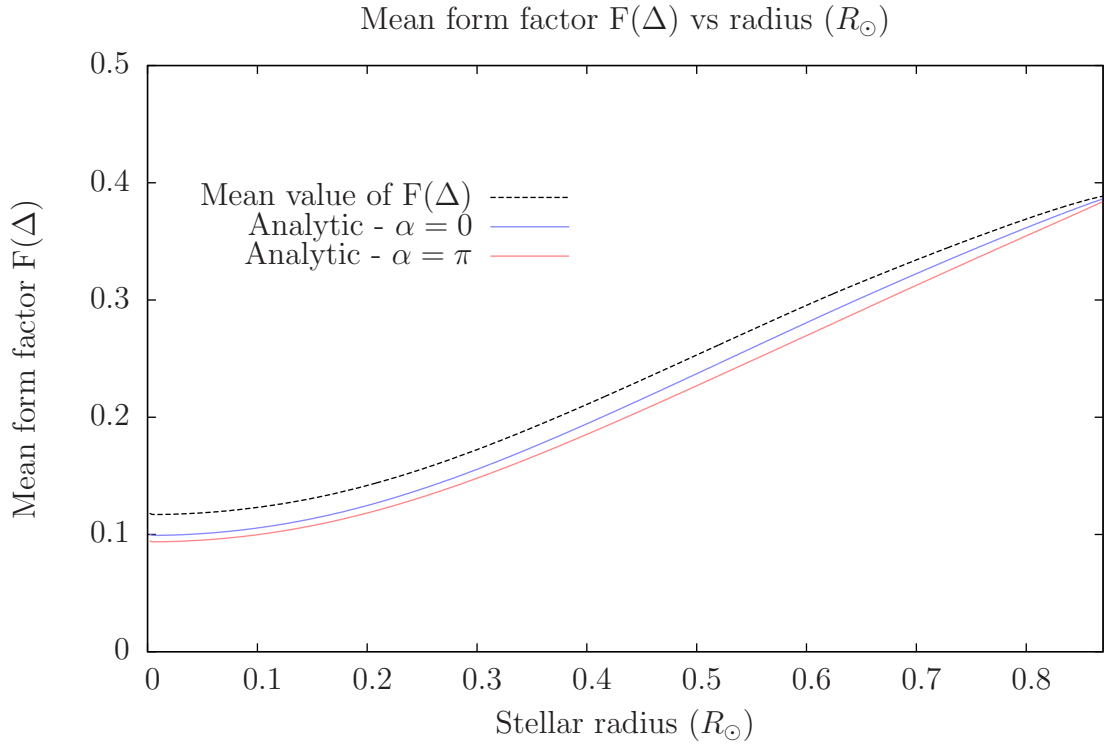

Figure 2.6: Form factor of iron as as a function of r. The form factor is computed analytically for $\alpha \equiv 0$ and $\alpha \equiv \pi$. The mean value of $F(\Delta)$ (averaged over all α) is also shown. This plot shows that the simplification $\alpha \equiv 0$ gives reasonable values for $F(\Delta)$ even in the worst case scenario of a WIMP colliding with iron at the centre of the star.

It should also be noted that the WIMP mass density and the collision cross section are highly uncertain. Hence, any results from this project can only be considered magnitude estimates. Given the approximation $\alpha \equiv 0$, equations 2.5, 2.7 and 2.9 simplify to (Appendix A):

$$\boldsymbol{v}'_\chi = \left[u\left(\frac{m_\chi}{m_N} + \cos\theta\right) + v_N\right]\hat{\boldsymbol{i}} + u\sin\theta\,\hat{\boldsymbol{j}} \tag{2.13a}$$

$$\Delta = A(1-\cos\theta) \tag{2.13b}$$

$$F(\Delta) = e^{B(\cos\theta - 1)} \tag{2.13c}$$

Where:

$$u = \mu_N(v_\chi - v_N) \qquad w \equiv \frac{v_N}{v_\chi}$$

$$A \equiv 2\mu_N(1-w)(\mu_\chi + w\mu_N)$$

$$B \equiv \frac{E_\chi}{E_0}A$$

This approximation is chosen because it greatly simplifies equations 2.5, 2.7 and 2.9 while introducing only a modest error. The greatest risk is that an approximation might alter the nuclear scattering cross section of a WIMP. As we saw earlier, the nuclear scatter cross section for elements heavier than Hydrogen is:

$$\langle\sigma\rangle = \frac{\sigma_0}{2}\int F(\Delta)\cdot\sin\theta\; d\theta$$

The largest error in $\langle\sigma\rangle$ occurs for the heaviest element (iron) and the highest WIMP and nucleon speeds (i.e. a collision in the Sun's core). Even in this extreme case, the error introduced by fixing $\alpha \equiv 0$ is at most 17%. As we will see later, WIMP capture is dominated primarily by Hydrogen, and secondly by Helium and Oxygen, so that the approximation $\alpha = 0$ introduces a negligible error in all relevant calculations.

2.4.1 Probability distributions (revised)

In order to calculate P_{col} (Equation 2.11) and P_θ (Equation 2.12) it is necessary to compute the integral $\int F(\Delta)\sin\theta d\theta$. Thanks to the approximation ($\alpha = 0$) this integral can be solved analytically (Appendix A):

$$\int_0^\pi F(\Delta)\;\sin\theta\; d\theta = \frac{1-e^{-2B}}{B}$$

With this, the probability distributions (Equations 2.11 and 2.12) become:

$$P_{col} = \sum_j n_j(r)\,\langle\sigma_j\rangle \tag{2.14a}$$

$$P_\theta = \frac{B\,e^{B\cos\theta}\sin\theta}{e^B - e^{-B}} \tag{2.14b}$$

Where:

$$\langle\sigma_H\rangle \equiv \sigma_{SD} \qquad \text{(Hydrogen)}$$

$$\langle\sigma_j\rangle \equiv \sigma_{SI}\left(\frac{m_j(m_\chi + m_H)}{m_H(m_\chi + m_j)}\mathcal{A}\right)^2 \cdot \frac{1 - e^{-2B}}{2B} \qquad \text{(Other elements)}$$

Figure 2.7 shows the mean cross section $\langle\sigma_j\rangle$ for some nuclear elements. As in previous figures, this is for a 100 GeV WIMP travelling at escape velocity. Figure 2.8 shows P_θ for a 100 GeV WIMP at escape velocity at $r = 0$. Helium is not shown because its distribution is almost identical to hydrogen's. Notice that as the nucleus mass grows, the probability distribution is shifted toward smaller θ, since larger θ involves higher momentum transfer, which is suppressed by the form factor.

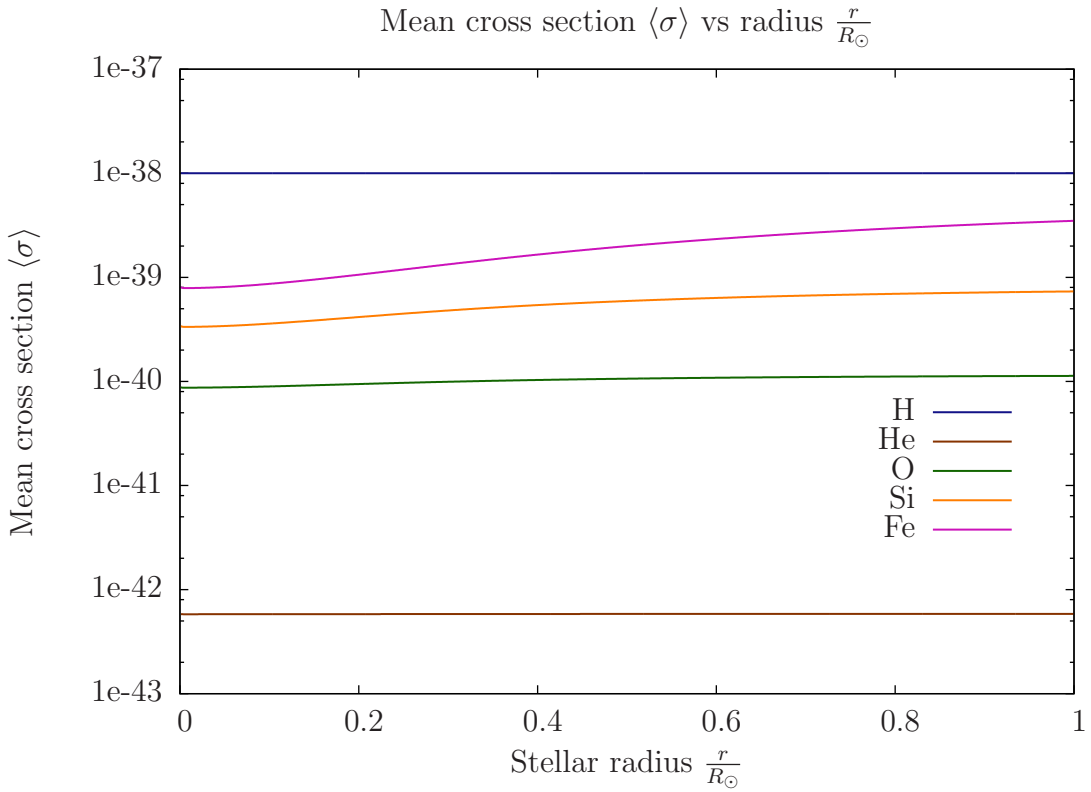

Figure 2.7: Mean nuclear scattering cross section $\langle\sigma\rangle \equiv \frac{\sigma_0}{2}\int F(\Delta)\cdot\sin\theta\;d\theta$ for a WIMP and an atomic nucleus. The WIMP has a mass of 100 GeV and travels at escape velocity inside the Sun. The scatter cross section is written in units of cm^2.

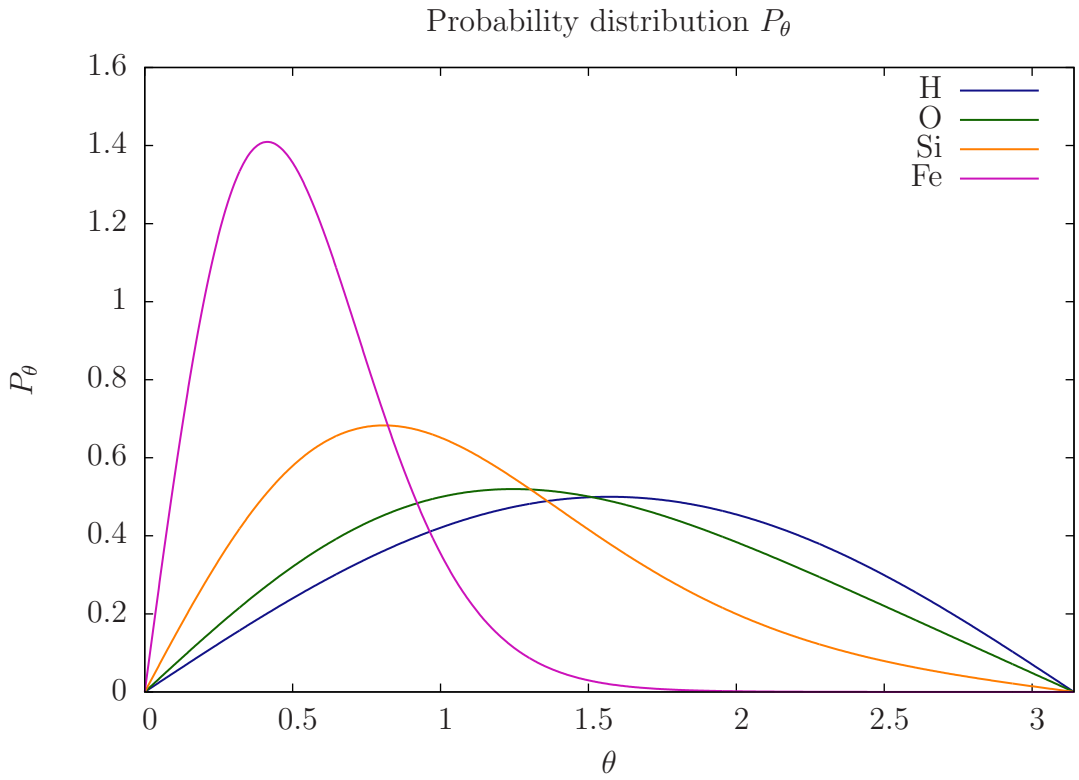

Figure 2.8: Probability distribution P_θ of the scatter angle θ in the centre of mass frame. For heavier nuclei, the distribution is shifted toward small θ, since the form factor suppresses the scatter cross section σ for larger angles.

2.4.2 Solar model and P_{col}

The calculation of P_{col} requires a standard solar model that gives the particle density $n_j(r)$ at various points in the star. I used the zero-age solar model produced by the STARS code which was originally written by Eggleton (1971) and was extensively modified by Pols et al. (1995).

Since this solar model only contains abundances for ^{1}H, ^{4}He and ^{12}C, I complemented it with a table of initial solar abundances from Anders & Grevesse (1989) and applied the following assumptions:

- Since the CNO cycle mainly affects the abundance of ^{12}C and ^{14}N, I assume that any depletion of ^{12}C in the Sun implies a corresponding increase in ^{14}N.
- I assume that the abundances of all elements besides ^{1}H, ^{4}He, ^{12}C and ^{14}N are uniform and unchanged from the Sun's initial state.

In this way I obtain reasonable estimates for the abundance of most elements inside the Sun. Figure 2.9 shows the probability of collision P_{col} for the seven most important elements in the Sun. As before, this is for a 100 GeV WIMP at escape velocity. Compare this figure with Figure 2.7. The difference reflects the changes in density and composition inside the Sun.

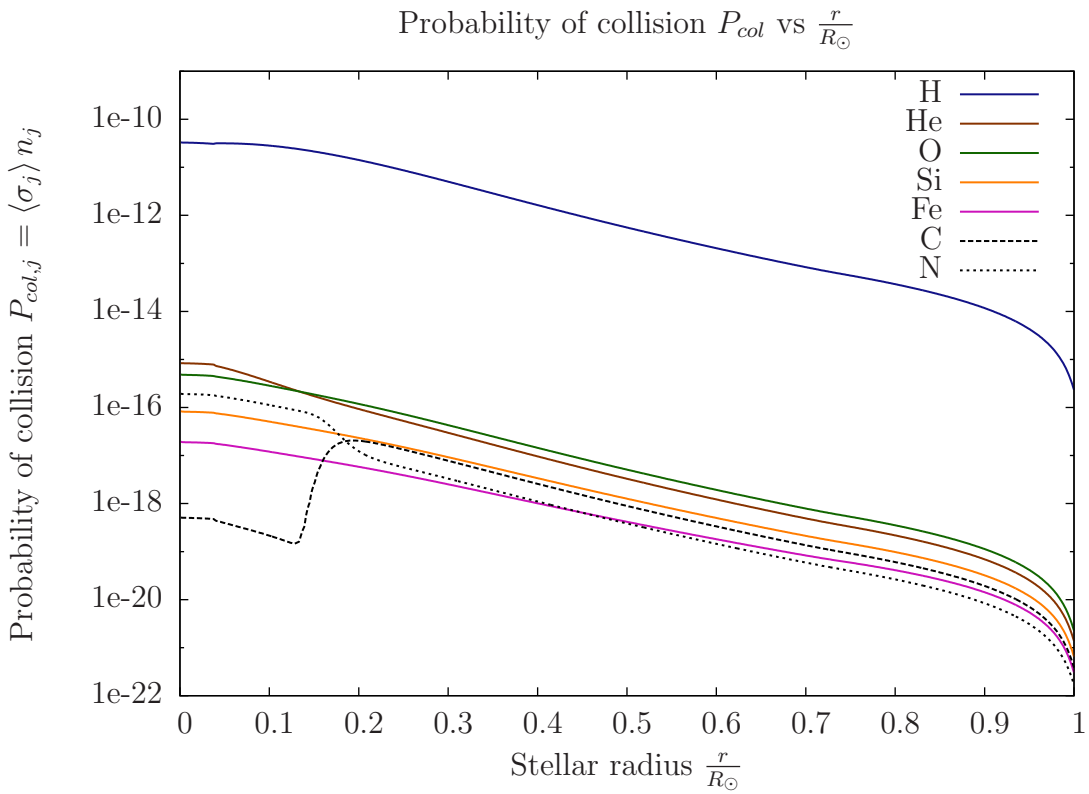

Figure 2.9: Probability of collision *per meter* for the seven most important elements in the Sun. As shown in Equation 2.14a, this probability is a function of the local number density of each atomic element and the WIMP-nucleus scatter cross section for that element. Notice, for example, that the probability of collision with carbon drops dramatically inside the Sun's core. This is because the CNO cycle has mostly depleted the local carbon nuclei by converting them into nitrogen.

Chapter 3

Capture rate for a single star

3.1 Introduction

Before attempting to solve the complex problem of WIMP capture in a binary system, it is good to attempt a simpler problem: WIMP capture by a single star, without a companion is simpler, and has been studied by previous research (e.g. Scott et al., 2009).

3.2 Partial probability of capture

For a single star, capture is easy to define: A WIMP is captured when its velocity is less than the escape velocity. If v_∞ is the speed of the WIMP away from the Sun, the local speed is $v_\chi = \sqrt{v_\infty^2 + v_e^2}$. For capture, the fractional energy loss Δ must be at least:

$$\Delta_{min} = \frac{v_\infty^2}{v_e^2}$$

Recall that $\Delta = A(1-\cos\theta)$ (Equation 2.13b). If $\Delta_{min} > 2A$, capture is not possible, otherwise, the probability that a collision results in capture can be derived from P_θ (Equation 2.14b):

$$A(1-\cos\theta) > \Delta_{min} \Rightarrow \theta > \arccos\left(1 - \frac{\Delta_{min}}{A}\right)$$

$$\therefore \theta_{min} \equiv \arccos\left(1 - \frac{\Delta_{min}}{A}\right)$$

The probability that a collision results in capture is $P_\theta(\theta > \theta_{min})$. For hydrogen that becomes:

$$P_{\theta,H}(\theta > \theta_{min,H}) = \frac{1}{2}\int_{\theta_{min,H}}^{\pi} \sin\theta d\theta = \frac{1+\cos\theta_{min,H}}{2} = 1 - \frac{\Delta_{min}}{2A}$$

And for other elements:

$$P_{\theta,j}(\theta > \theta_{min,j}) = \frac{B_j}{e^{B_j} - e^{-B_j}} \int_{\theta_{min,j}}^{\pi} e^{B_j \cos\theta} \sin\theta d\theta = \frac{e^{B_j \cos\theta_{min,j}} - e^{-B_j}}{e^{B_j} - e^{-B_j}}$$

Combining this with the probability of collision P_{col} (Equation 2.14a) gives the probability of capture over a small path element ds:

$$\begin{aligned} \mathrm{d}P_{cap} &= \sum_j P_{col,j} P_{\theta,j}(\theta > \theta_{min,j}) \mathrm{d}s \\ &= \sum_j n_j \langle \sigma_j \rangle P_{\theta,j}(\theta > \theta_{min,j}) \mathrm{d}s \\ &= n_H \sigma_H \left(1 - \frac{\Delta_{min}}{2A}\right) \mathrm{d}s + \sum_{j \neq H} n_j \sigma_{0,j} \frac{1 - e^{-2B_j}}{2B_j} P_{\theta,j}(\theta > \theta_{min,j}) \mathrm{d}s \end{aligned}$$

Where $\sigma_{0,j}$ is defined in Equation 2.8 and $\sum_{j \neq H}$ denotes a sum over elements other than Hydrogen.

Let $\mathcal{E} = \frac{E_\chi}{E_0}$ and after a little algebra the formula for dP_{cap} simplifies to:

$$\frac{\mathrm{d}P_{cap}}{\mathrm{d}s} = n_H \sigma_H \left(1 - \frac{\Delta_{min}}{2A_H}\right) + \sum_{j \neq H} n_j \sigma_{0,j} \cdot \frac{e^{-\mathcal{E}_j \Delta_{min}} - e^{-2B_j}}{2B_j} \tag{3.1}$$

Figure 3.1 shows dP_{cap} in units of probability of capture per meter for a WIMP going through the Sun. Notice that the shape of the curves resemble the ones from Figure 2.9 (probability of collision).

Notice that for $v_\infty = 125$, 150 and 175 km s^{-1} there is a sudden drop part-way through the Sun. The reason for this is a little subtle: hydrogen normally dominates WIMP capture, but the ability of hydrogen to capture WIMPs is limited by the momentum of the hydrogen nuclei. As we move away from the Sun's core, the temperature drops very rapidly, and with that the speed of hydrogen nuclei. At some point, the hydrogen nuclei cannot transfer enough momentum to the WIMP to slow it below escape velocity. At this point, hydrogen becomes incapable of capturing WIMPs, and capture is then dominated by helium and oxygen.

This is also the reason behind the shape of the $v_\infty = 200$ km s^{-1}. For WIMPs travelling that fast, hydrogen nuclei cannot transfer enough momentum to a WIMP to slow it below escape velocity. For WIMPs travelling at 200 km s^{-1} or faster, only heavier elements can capture WIMPs, so that for these WIMPs the capture rate will be practically zero.

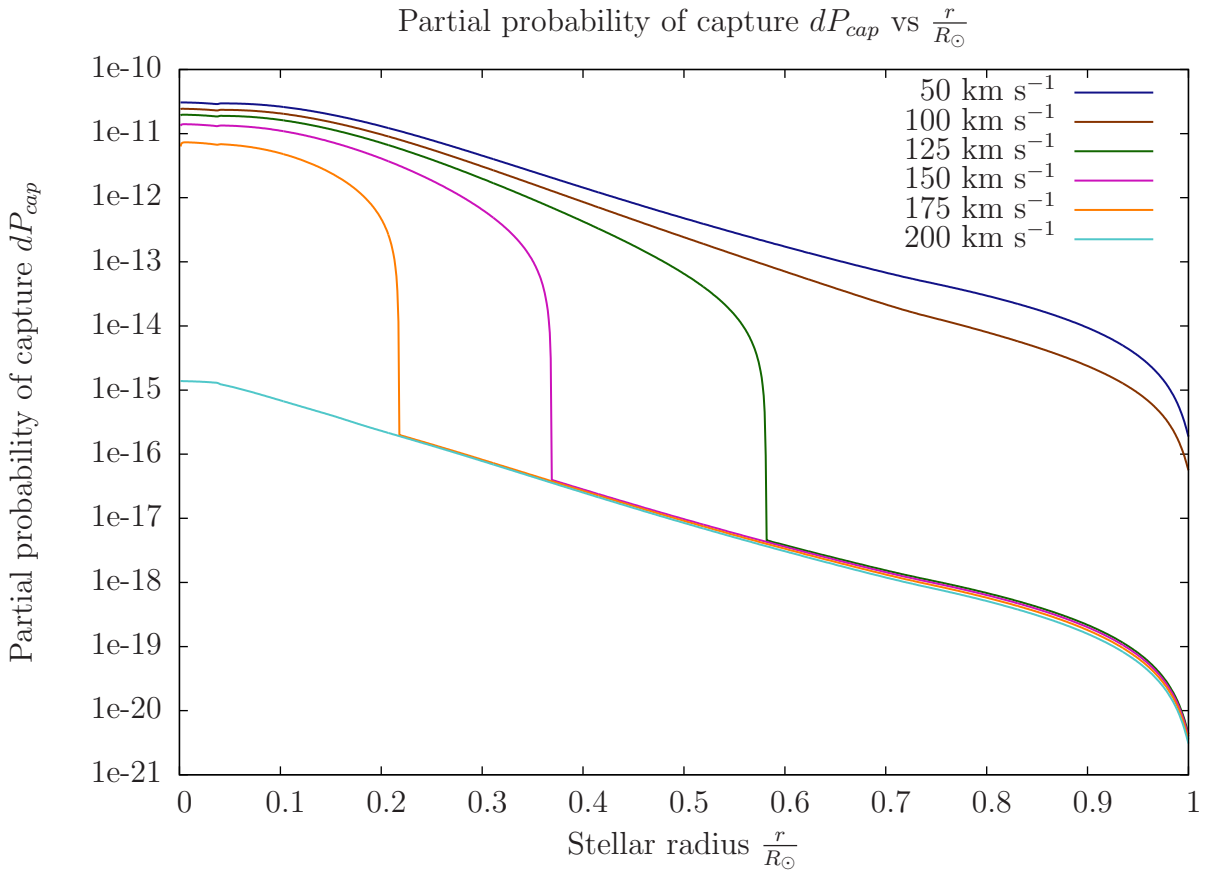

Figure 3.1: Probability of capture *per meter* for different values of v_∞.

3.3 Path of a WIMP through the star

To compute the total probability of capture as a WIMP travels through the Sun, we integrate $\mathrm{d}P_{cap}$ along the path of the WIMP inside the Sun.

- Let r_p and v_p be the velocity of the WIMP at perihelion. If v_e is the escape velocity at r_p then $v_p = \sqrt{v_e^2 + v_\infty^2}$ where v_∞ is the speed of the WIMP at infinity.
- Let b be the *perpendicular distance* between the WIMP's position at infinity and the centre of the Sun. This is best understood via the illustration in Figure 3.2.

Note that, "at infinity", the WIMP angular momentum is $J = \|\boldsymbol{r}_\infty \times \boldsymbol{p}_\infty\| = b \cdot (m_\chi\, v_\infty)$, where $\boldsymbol{r}_\infty$ is the position vector of the WIMP relative to the Sun's centre. At perihelion, the angular momentum is $J = r_p \cdot (m_\chi\, v_p)$. By conservation of angular momentum, we obtain the relation:

$$b \cdot v_\infty = r_p \cdot v_p \qquad \text{where} \quad v_p = \sqrt{v_e(r_p)^2 + v_\infty^2} \tag{3.2}$$

Therefore, for any choice of (v_∞, r_p) we can obtain b and v_p. Starting with (r_p, v_p), we can compute the WIMP's path. With this, we can now integrate $\mathrm{d}P_{cap}$ numerically over the path

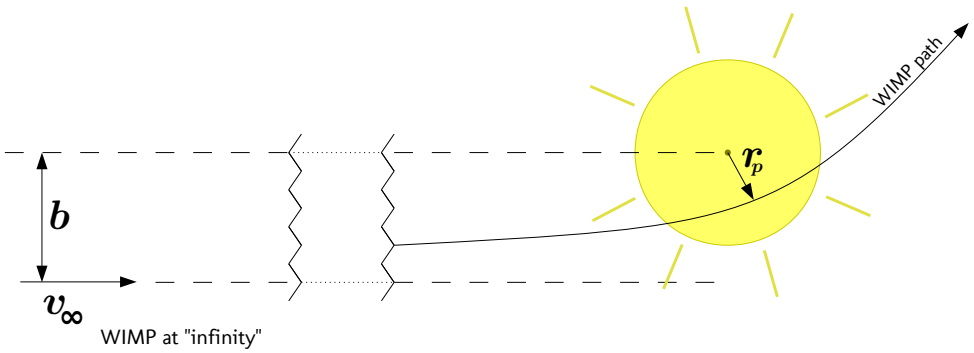

Figure 3.2: The path of a WIMP through the Sun can be parametrized by b and v_∞.

of the WIMP through the Sun to obtain the total probability of capture. Since the path of the WIMP is parametrized by r_p and v_∞, we write P_{cap} as:

$$P_{cap}(r_p, v_\infty) = \int_{s(r_p, v_\infty)} \frac{\mathrm{d}P_{cap}}{\mathrm{d}s} \mathrm{d}s$$

Figure 3.3 shows P_{cap} vs r_p for various choices of v_∞.

3.4 Capture cross section σ_{cap}

We can summarize the information contained in P_{cap} with a "capture cross section" σ_{cap} as:

$$\sigma_{cap}(v_\infty) \equiv \int_0^{b_{max}} 2\pi\, b\, P_{cap}\, \mathrm{d}b \tag{3.3}$$

This is in some ways analogous to the WIMP-nucleus cross section. It summarizes the probability that a WIMP of speed v_∞ will be captured by the Sun. Using Equation 3.2 we write:

$$b = \left(\frac{v_p}{v_\infty}\right) r_p \qquad \text{and} \qquad \mathrm{d}b = \left(\frac{v_p}{v_\infty}\right) \mathrm{d}r_p$$

$$\therefore \sigma_{cap}(v_\infty) = \int_0^{R_\odot} 2\pi \left(\frac{v_p}{v_\infty}\right)^2 r_p\, P_{cap}(r_p, v_\infty)\, \mathrm{d}r_p$$

Table 3.1 shows some sample values for σ_{cap}. At first sight the values of σ_{cap} might seem surprisingly large for slow moving WIMPs (e.g. $\sigma_{cap} = 4.7 \times 10^{17}$ m^2 $= 0.972\ R_\odot^2$ for $v_\infty = 50\,\mathrm{km\,s^{-1}}$). Recall that slow-moving WIMPs have a large range of possible impact parameters (e.g. $b_{max} \gtrsim 12 R_\odot$ for $v_\infty = 50\,\mathrm{km\,s^{-1}}$), which greatly increases the value of the integral in Equation 3.3.

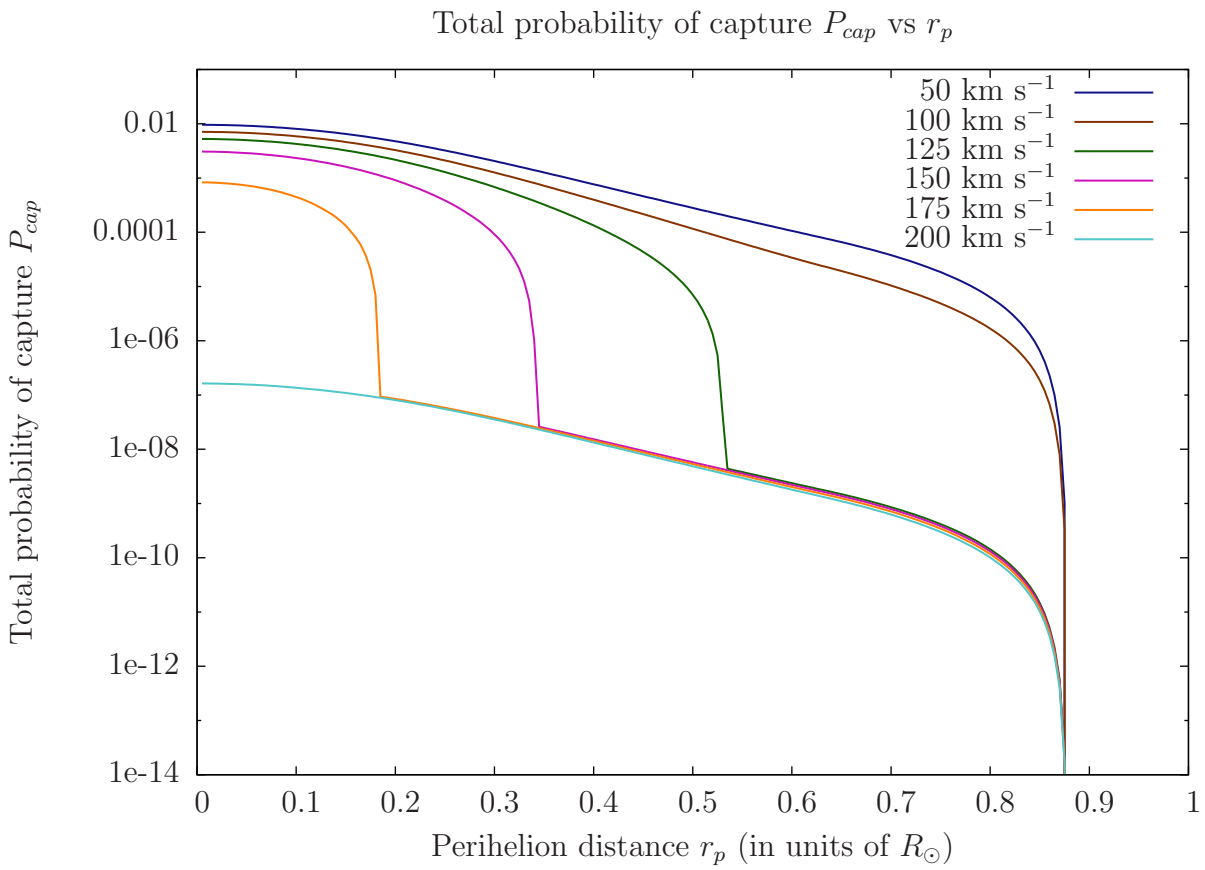

Figure 3.3: Cumulative probability of capture over the entire WIMP path as a function of r_p. This plot was produced using a model of the zero-age Sun. When the Sun was first formed, it had a smaller radius than it does today. This is why the probability of WIMP capture drops to zero at about $r = 0.87 R_\odot$.

Table 3.1: Sample values of σ_{cap} for a $1 M_\odot$ zero-age Sun.

v_∞	$\sigma_{cap}(v_\infty)$
50 km s^{-1}	4.7×10^{17} m^2 $= 0.972\ R_\odot^2$
100 km s^{-1}	8.2×10^{16} m^2 $= 0.170\ R_\odot^2$
125 km s^{-1}	3.5×10^{16} m^2 $= 0.072\ R_\odot^2$
150 km s^{-1}	1.2×10^{16} m^2 $= 0.025\ R_\odot^2$
175 km s^{-1}	2.1×10^{15} m^2 $= 0.004\ R_\odot^2$
200 km s^{-1}	5.9×10^{11} m^2 $= 1.2 \times 10^{-6} R_\odot^2$

3.5 Capture rate

Equipped with σ_{cap}, we can now express the WIMP capture rate as:

$$C = \int_{v_\infty} \sigma_{cap}(v) v\ n_\chi\ f(v) \mathrm{d}v$$

Where $n = \rho_\chi / m_\chi$ is the ambient WIMP number density and $f(v)$ is the WIMP velocity distribution. Note that $\sigma_{cap}(v)v$ has units of volume per unit time, so that $\sigma_{cap}(v)v\ n$ and C have units of WIMP number per unit time. We saw in section 1.5.2 that in the star's reference frame, the WIMP speed distribution follows equation 1.4 which is reproduced below:

$$f_\star(v_\infty) = f_0(v_\infty) \exp\left(\frac{-3v_\star^2}{2\overline{v}^2}\right) \frac{\sinh(3v_\infty v_\star/\overline{v}^2)}{3v_\infty v_\star/\overline{v}^2}$$

Where v_∞ is the WIMP speed before it is affected by the star's gravity, $\overline{v}$ is the velocity dispersion and $v_\star$ is the star's speed in the galaxy. One can approximate the local velocity dispersion in terms of $v_\star$ with $\overline{v} \approx v_\star\sqrt{3/2}$, so that the capture rate becomes:

$$f_\star(v_\infty) = \frac{2}{\sqrt{\pi}} \frac{v_\infty}{v_\star^2} \exp\left(-\frac{v_\infty^2 + v_\star^2}{v_\star^2}\right) \sinh\left(\frac{2v_\infty}{v_\star}\right)$$

$$\therefore C_\star = \frac{2\,n_\chi}{\sqrt{\pi}} \int_{v_\infty} \sigma_{cap}(v) \frac{v^2}{v_\star^2} \sinh\left(\frac{2v}{v_\star}\right) e^{-(v^2/v_\star^2+1)} \mathrm{d}v$$

3.5.1 WIMP number density n_χ

As mentioned in section 1.5.2, WIMPs are thought to lie in a spherical halo with a density profile that increases the WIMP density close to the galactic centre. WIMP halos are typically modelled as a series of power laws $\rho_\chi \propto r^\gamma$ where γ varies with distance to the galactic centre. For example, Scott et al. (2009) considered two WIMP density profiles:

$$\begin{array}{lll} \rho_\chi(r) = & \rho_\chi(100\text{ pc})\left(\frac{100\text{ pc}}{\text{r}}\right)^{\gamma_1} & r > r_{out} \\ \rho_\chi(r) = & \rho_\chi(r_{out})\left(\frac{r_{out}}{r}\right)^{\gamma_2} & r_{out} > r > r_{in} \\ \rho_\chi(r) = & \rho_\chi(r_{in}) & r < r_{in} \end{array}$$

Table 3.2: Sample WIMP density profiles

	$\rho_\chi(100\text{ pc})$	γ_1	γ_2	r_{out}	r_{in}
Model 1	25 GeV cm^{-3}	1	1.85	$7 \times 10^4 R_{BH}$	$10R_{BH}$
Model 2	360 GeV cm^{-3}	1.5	1.82	$7 \times 10^4 R_{BH}$	$10R_{BH}$

Figure 3.4 shows these two profiles. Observe that for S-stars orbiting the central galactic black hole the WIMP mass density is as high as $\rho_\chi = 10^{12}$ GeV cm^{-3} to $\rho_\chi = 10^{15}$ GeV cm^{-3} depending on the model, while in the solar neighbourhood the WIMP density is a mere $\rho_\chi \sim$ 1 GeV cm^{-3}.

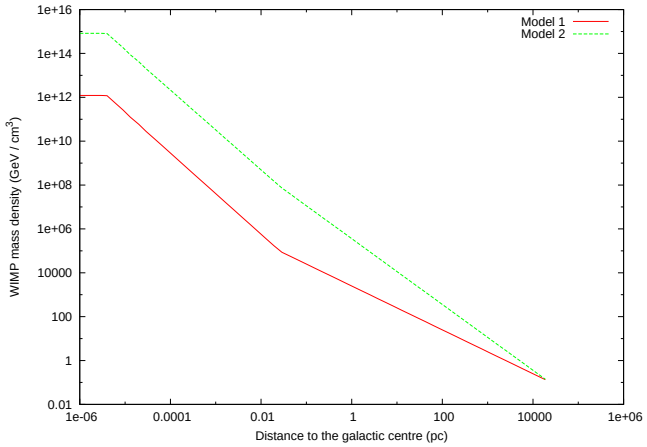

Figure 3.4: The WIMP density profile (i.e. WIMP mass density versus distance from the galactic centre) is uncertain. This figure shows two sample models of what the density profile might look like.

In the work of Scott et al. (2009), the team uses a "Reference Solar Configuration" (RSC) which consists of a solar velocity distribution ($v_\star = 220$ km s^{-1}, $\overline{v} = 270$ km s^{-1}) and a WIMP density profile in the region of $\rho_\chi = 10^{10}$ GeV cm^{-3}. To facilitate comparison with Scott et al. (2009), this thesis uses this same RSC, but it is important to observe in Figure 3.4 that these parameters do not correspond to any realistic stellar orbit.

Consider a star orbiting the galactic black hole with a Sun-like speed of $v_\star = 200$ km s^{-1}. Given a black hole mass of $M \sim 4 \times 10^6 M_\odot$, this orbit corresponds to $r \approx 0.355$ pc. The corresponding WIMP densities for models 1 and 2 (Table 3.2) are shown in Table 3.3, along with the RSC value. Notice that the WIMP density is highly uncertain, and in any case is much lower than the RSC value used by Scott et al. (2009).

Table 3.3: Background WIMP density for models 1 and 2 (Table 3.2) and the Reference Solar Configuration (RSC)

	$v_\star = 220$ km s^{-1}
RSC	$\rho_\chi \equiv 10^{10}$ GeV cm^{-3}
Model 1	$\rho_\chi = 7.0 \times 10^3$ GeV cm^{-3}
Model 2	$\rho_\chi = 1.7 \times 10^6$ GeV cm^{-3}

3.5.2 Comparison with previous work

Equipped with a WIMP number density n_χ it is now possible to obtain a capture rate. In the Reference Solar Configuration ($v_\star = 220$ km s^{-1}, $\overline{v} = 270$ km s^{-1} and $\rho_\chi = 10^{10}$ GeV cm^{-3}) and for a $1 M_\odot$ zero-age star, the capture rate is:

$$C_\star = 2 \times 10^{42} \quad \text{WIMPs/year} \qquad \text{(for 100 GeV WIMPs)}$$

To compare this result with the work of Scott et al. (2009) one must turn to Figure 2 of their paper. This figure presents the WIMP capture rate as a function of $\log_{10}(\rho_\chi \sigma_{SD}/\overline{v})$. For the Reference Solar Configuration, and a cross section $\sigma_{SD} = 10^{-38}$ cm^2 (see section 1.4.4 for discussion of σ_{SD}) one obtains:

$$\log_{10}\left(\frac{\rho_\chi \sigma_{SD}}{\overline{v}}\right) = -35.431$$

This corresponds to a capture rate of $C \sim 3 \times 10^{39}$ WIMPs / yr for a $1M_\odot$ zero-age star. There is an obvious discrepancy here: The capture rate from my simulation is about 1000 times greater than that obtained by Scott et al. (2009).

I attempted to find the source of this discrepancy without success. One difference between this work and Scott et al. (2009) is that they use a WIMP mass of $m_\chi = 60$ GeV/c^2 while this work uses $m_\chi = 100$ GeV/c^2. But that change only serves to slightly increase WIMP number density and with that, the nominal capture rate (see Table 3.4).

Table 3.4: Capture rate (WIMPs / year) for various models.

	Capture Rate
100 GeV WIMPs	2×10^{42}WIMPs/yr
60 GeV WIMPs	3×10^{42}WIMPs/yr
Scott et al. (2009)	3×10^{39}WIMPs/yr

When converted to 60 GeV WIMPs, the capture rate from my simulation differs from that of Scott et al. (2009) by a clean factor of 1000. This conspicuous difference suggests a scaling error (e.g. mixing kilometers and meters somewhere) but a careful review of the simulation did not reveal any such error. Likewise, a review of Scott et al. (2009) did not reveal errors with their work either. In the end, it was decided that it is beyond the scope of the thesis to investigate the origin of this discrepancy in detail.

The WIMP capture rate can be expressed as a luminosity: When the star reaches equilibrium, the WIMP annihilation rate will exactly balance the capture rate ($C = 2A$). A capture rate of $3\times10^{42}\times(60$ GeV)/yr gives a luminosity of $2.6L_\odot$, while a capture rate of $3\times10^{39}\times(60$ GeV)/yr gives a luminosity of $0.0026L_\odot$. The take-away message is that $0.0026L_\odot$ is not significant for a $1M_\odot$ star, while $2.6L_\odot$ is.

Chapter 4

N-body simulation

Unfortunately, the semi-analytic approach used in the previous chapter cannot be extended to binary systems. The gravitational interaction from two massive stars will affect WIMP orbits in complicated ways. Therefore, it is necessary to develop an N-body simulation that directly models WIMP capture.

The N-body simulation would start with the stellar binary centred at the origin, and several thousand WIMPs (test particles) at some large distance from the binary. The simulation needs to follow the trajectories of WIMPs as they move in the gravitational field of the binary system. It also needs to keep track of collisions between WIMPs and atomic nuclei.

An N-body simulation is more complex and more error prone than the semi-analytic calculation from the previous chapter. In this chapter, I develop an N-body simulation *for a single star*, and use it to reproduce the results from the previous chapter. This is an important step to *validate* the technique and the numerical code before attempting a binary simulation.

4.1 Simulation design

4.1.1 WIMP distribution

The first step is to produce a pseudo-random number generator (PRNG) to produce WIMPs with the correct velocity distribution. These velocities serve as part of the initial conditions for the N-body simulator to be developed next.

To accomplish this, WIMP velocities are first generated in the galactic reference frame (Equation 1.3). In this reference frame it is simple to choose the WIMP's velocity vector as all directions are equally likely. The WIMP velocity is then changed to the reference frame of the star (for the single star simulation) or the binary centre of mass (for the binary simulation). I have confirmed that the resulting WIMP speeds follow the distribution in Equation 1.4. This approach ensures that the WIMPs have not only the correct speed distributions, but that the directions of the WIMPs are correct also. This level of detail is not needed for the single star simulation, but it may be relevant for the binary simulation.

One important detail is that the WIMP distribution that the star receives per unit of time goes with $v_\infty \cdot f_\star(v_\infty)$ rather than $f_\star(v_\infty)$. To account for this, I modified the WIMP generator to accept or reject WIMPs with probability $P \propto v_\infty$.

4.1.2 N-body integrator

One of the biggest concerns in this simulation is numerical accuracy. The simulation needs to model orbits that are very eccentric, with orbital energies very close to zero, and the orbits will be modelled over many years. Hence, it is easy for numerical errors to build up and incorrectly capture or eject WIMPs.

In order to minimize this concern, I wrote a Gragg-Bulirsch-Stoer (GBS) integrator instead of the simpler Runge-Kutta 4 (Press et al., 2002). The GBS algorithm is fairly complex and difficult to implement correctly, but it tends to give better solutions in situations where numerical accuracy is important. The GBS method is not a symplectic (energy-preserving) algorithm, but it is derived from the symplectic leap-frog method, and so it inherits good energy-preserving properties.

For the orbits to be correct, the Sun has to be modelled as a distributed mass. I use a zero-age model of the Sun (ZAMS) to remain consistent with the work of Scott et al. (2009). However, GBS is very sensitive to the smoothness of the function being integrated. For this reason, it was necessary to approximate mass inside the Sun with a polynomial. The polynomial is designed such that the gravitational force is twice-differentiable at the boundary of the star. The polynomial was produced with the help of Maxima[1]:

$$m(x) \approx \frac{6622}{117}x^3 - \frac{23831}{117}x^4 + \frac{3802}{13}x^5 - \frac{22612}{117}x^6 + \frac{440}{9}x^7 \qquad \text{where } x \equiv \frac{r}{R_\star} \tag{4.1}$$

One of the best ways to test the quality of an N-body simulation is to measure conservation of energy. All numerical simulations incur some error which is reflected in the particle's total energy. The Runge-Kutta family of integrators has a tendency to steadily lose energy, possibly causing particles to erroneously become bound to the system. Symplectic integrators have a tendency to lose energy in one half of the orbit and gain it in the other half. Since GBS is based on an symplectic integrator, it can produce both energy gain and energy loss.

I tested the GBS integrator on a handful of WIMPs with typical velocities. The test simulation simulation first records the initial energy of each WIMP $\mathcal{E}_0 = \frac{1}{2}v_\infty^2$. The WIMPs start at $5R_\odot$ and are allowed to move in the gravitational field of a single star, and at every time step the simulation computes the total WIMP energy $\mathcal{E} = \frac{1}{2}v^2 - \frac{GM}{r}$ as well as the loss or gain in energy:

$$\Delta\mathcal{E} = \mathcal{E} - \mathcal{E}_0$$

The test was performed both with and without the polynomial approximation (Equation 4.1). The results are shown in Figure 4.1. Each WIMP is represented with a different colour. For each

[1] http://andrejv.github.com/wxmaxima/

WIMP, there are three lines: The solid line (bottom) is the inbound trajectory, the thick dashed line (middle) is the outbound journey using the polynomial approximation (Equation 4.1), and the thin dotted line (top) is the outbound journey *without* the polynomial approximation. Notice that initially the error is very small ($\|\Delta\mathcal{E}/\mathcal{E}_0\| < 10^{-12}$) and only grows after crossing the star. This highlights the numerical difficulty of simulating particles inside a distributed mass and in strong gravitational fields. Conspicuously, Figure 4.1 does not include an error measurement inside the star. This is because it is very difficult to correctly compute the potential energy inside a distributed mass. The error in that calculation is greater than the simulation error that is being measured.

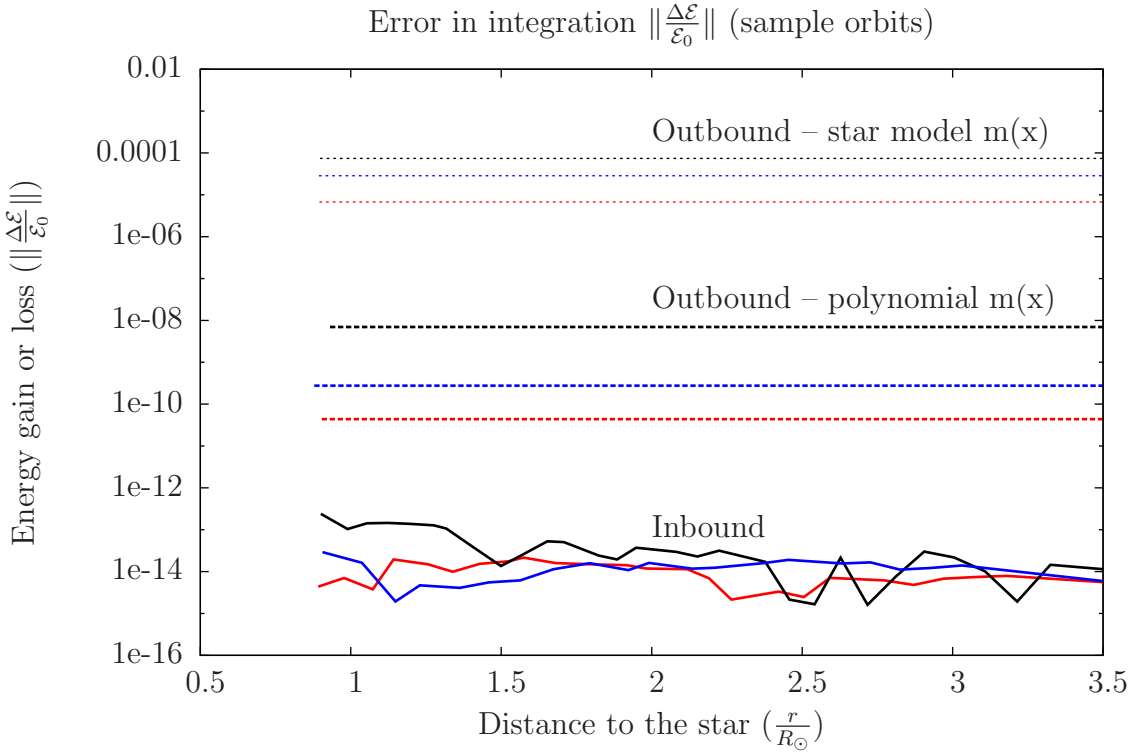

Figure 4.1: Energy error in three sample WIMP orbits. Each colour represents a different WIMP. The solid line represents the inbound trajectory while the dashed and dotted lines represent the outbound trajectory, both using the star model directly to obtain the enclosed mass $m(x)$ or using the polynomial approximation. The figure shows that passage through the star is responsible for the entire error $\|\Delta\mathcal{E}/\mathcal{E}_0\|$. Furthermore, the polynomial approximation accumulates less error in each passing.

Using only the enclosed mass from the stellar model, the error after a single crossing can be as high as $\|\Delta\mathcal{E}/\mathcal{E}_0\| \sim 10^{-4}$. For a simulation where WIMPs may cross the star hundreds of times, the accumulated error is unacceptable. As will be shown later (Figure 4.3), an accumulated error of $\sim 1\%$ is comparable to the energy loss after a WIMP-nucleus collision and is easily enough to erroneously absorb or eject a WIMP in a barely bound orbit (such as those in Figure 4.5). In contrast, the polynomial approximation reduces the final error to $\|\Delta\mathcal{E}/\mathcal{E}_0\| < 10^{-8}$. Now it is possible to model a WIMP for 10^4 orbits without affecting the physics of the simulation. It is worth noting that the simulation needs to be designed with a margin of safety. A binary simulation is likely to be more prone to numerical error than a single star simulation - especially as one moves toward close binaries with high speeds and strong gravitational potentials.

4.1.3 Simplifications

The simulation contains two simplifications meant to improve the computational efficiency:

WIMP swarms: Each "WIMP" is treated as a swarm of 10^5 particles. This means that a single computed orbit can give many WIMP collisions. This makes it easier to fully explore the parameter space with only a manageable number of computed orbits.

Only hydrogen: The simulation only includes collisions with hydrogen atoms, while ignoring all other elements. Figures 2.9 and 3.1 indicate that heavier elements only contribute minimally to WIMP capture and can be safely ignored.

4.2 Results

The purpose of the single-star simulation is to validate the N-body simulation before it is used in a binary simulation. This section presents some of the results obtained. First, it is worth noting in Figure 4.2 that only a small fraction of WIMPs have a sufficiently low impact parameter b and v_∞ to go through the star at a capturable speed.

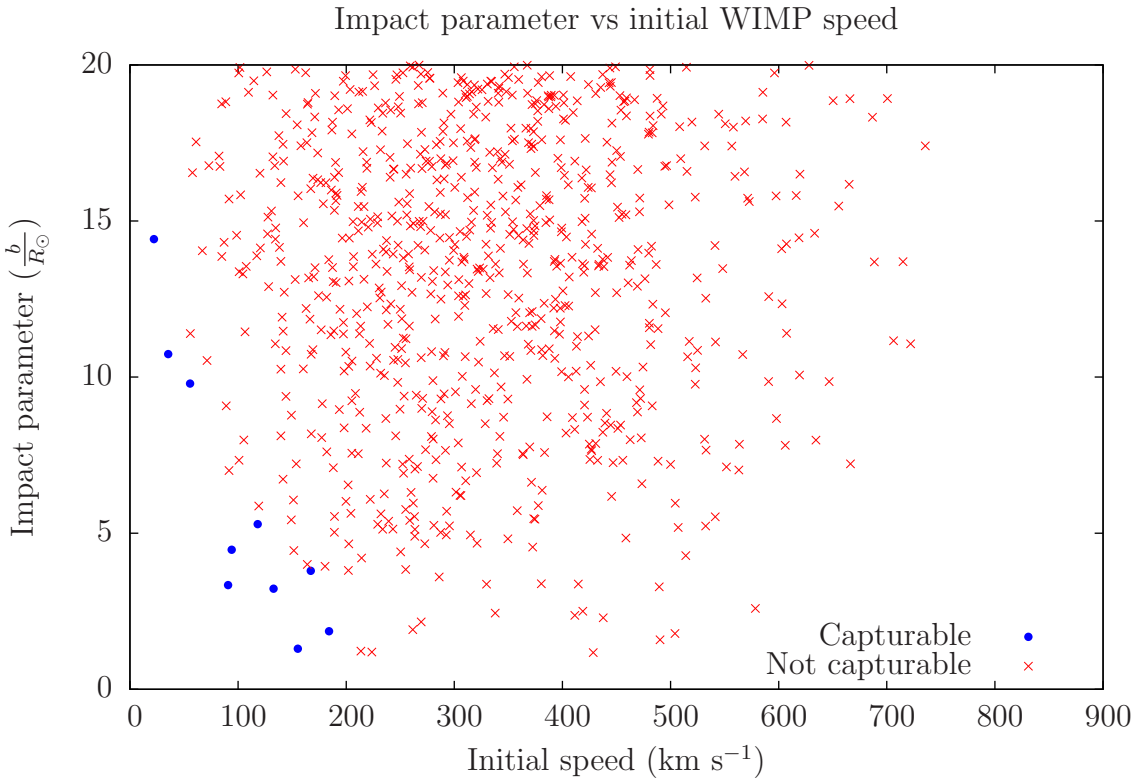

Figure 4.2: This plot shows a representative sample of the parameter space in terms of impact parameter and initial WIMP speed v_∞. Notice that most WIMPs have v_∞ in the order of a few hundred kilometres per second, as would be expected given the Sun's galactic speed of 200 km s^{-1}. Notice that the range WIMPs that are capturable (blue dots) constitute only a small fraction of the parameter space.

Figure 4.3 shows the kinetic energy lost after a WIMP-nucleon collision. As would be expected, WIMPs lose only a small fraction of their kinetic energy (up to $\sim 2\%$). This figure also shows that most collisions occur in the rough vicinity of $r = 0.2R_\odot$. This result is reasonable: on the one hand, WIMP collisions should be more common in the stellar regions with higher densities, but on the other hand, very few WIMP orbits go directly through the centre of the star - almost all WIMPs have a larger perihelion.

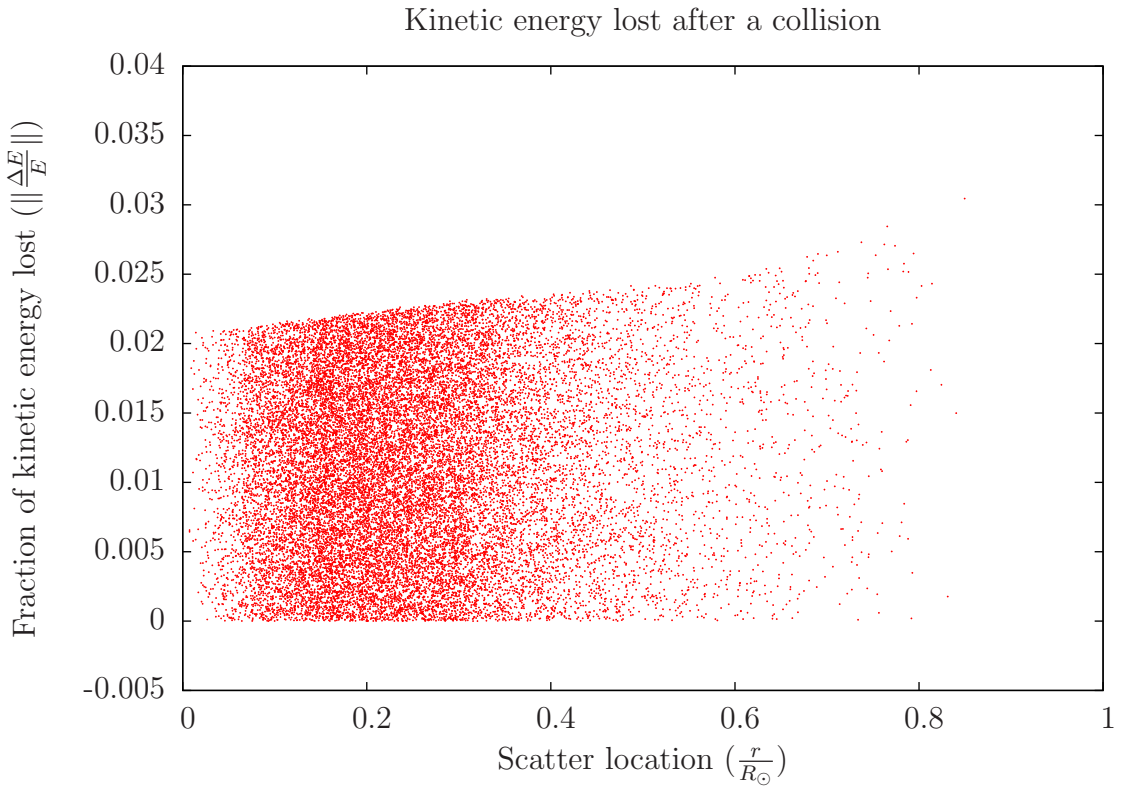

Figure 4.3: Kinetic energy lost after a collision. Observe that regardless of where the collision occurs, WIMPs lose in the order of $\sim 1\%$ of their kinetic energy. Furthermore, the loss in kinetic energy is almost never higher than $\sim 2.5\%$.

Figure 4.4 shows the (specific) WIMP binding energy $\mathcal{E}_b$ after a collision:

$$\mathcal{E}_b = -\mathcal{E} = -\frac{1}{2}v^2 - \mathcal{U}(r)$$

Where $\mathcal{U}(r)$ is the (specific) potential energy at r, which inside the star takes the form:

$$\mathcal{U}(r) = -\frac{GM_\star}{R_\star} - \int_{R_\star}^{r} \frac{GM(x)}{x^2} dx$$

Where $M(r)$ is the mass enclosed within radius r. Points with $\mathcal{E}_b < 0$ correspond to unbound orbits. Notice that WIMPs are universally captured with very low binding energies. The WIMPs are barely captured and have highly eccentric orbits. This is what one would expect for unbound particles that lose no more than $\sim 2\%$ of their kinetic energy.

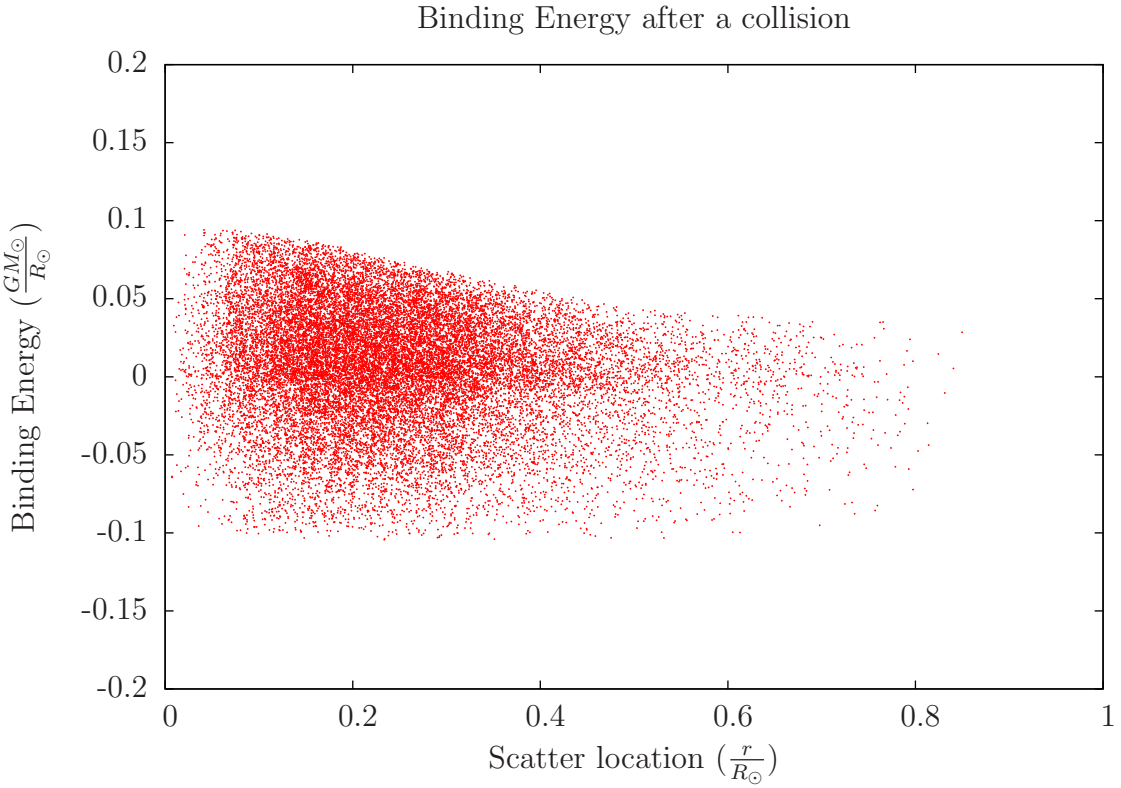

Figure 4.4: Binding energy after a collision. It is worth noting that the N-body simulation only includes WIMPs that are capturable (blue dots in Figure 4.2). This is why approximately half of the collisions in this plot result in capture (positive binding energy). Notice that binding energies are typically very low, corresponding to large semi-major axis (see Figure 4.5).

This point is also illustrated in Figure 4.5, which shows that the final WIMP orbits have very high eccentricities. Figure 4.5 also shows that the semi-major axis typically falls in the 5 to 200 $R_\odot$ range, which is in the same range as close stellar binaries. This means that there is a lot of opportunity to explore interesting physics in the final part of the project. Close binaries have orbital speeds comparable to the speed of stars around the galaxy, and they also have orbits in the same scale range as captured WIMPs. This means that the gravitational interaction of the two stars on the WIMP is what will ultimately determine whether WIMP capture is enhanced or suppressed by the binary system.

4.2.1 Capture Rate

Finally we come to the crux of the matter: Does the N-body simulation correctly reproduce the capture rate from the previous chapter? The answer is, "yes, it does". Table 4.1 shows the capture rate for both methods. Observe that the values agree within a factor of three.

This result is important: It validates the N-body simulation and it confirms that the work in the previous section is fundamentally sound (in spite of the disagreement with Scott et al. (2009)). Besides that, it is also worth noting that the N-body simulation appears to overestimate the capture rate. My investigations have failed to reveal the source of the discrepancy, but the discussion in section 4.1.2 seems to exonerate the GBS integrator as a likely culprit.

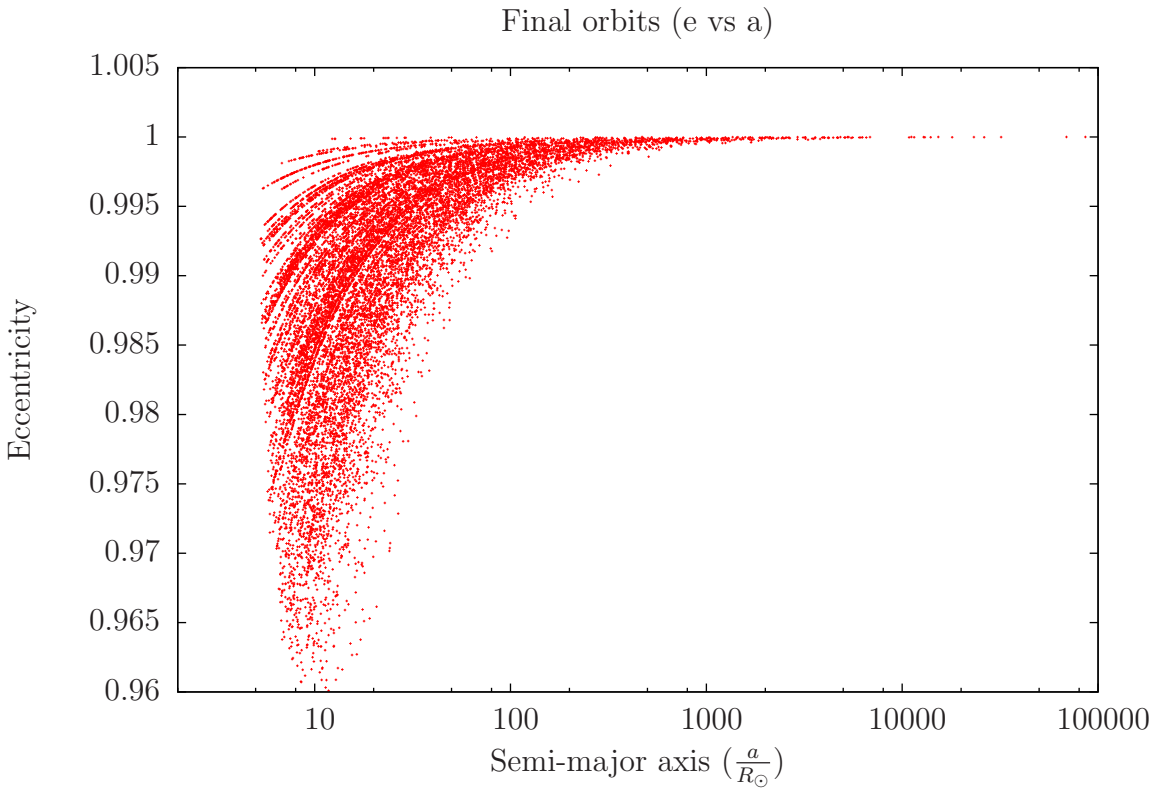

Figure 4.5: The orbital parameters of captured WIMPs after the initial collision. After the initial collision, bound WIMPs normally end up in highly eccentric orbits with large semi-major axis. WIMPs need to have additional collisions to be fully absorbed inside the star.

Table 4.1: Sample values for σ_{cap}

	Capture Rate
Semi-analytic method	$C = 1.97 \times 10^{42}$ WIMPs/year
N-body simulation	$C = 6.31 \times 10^{42}$ WIMPs/year

4.3 Conclusion

The key take-away message from this chapter is that the N-body simulation appears to give reasonable WIMP orbits and that it produces a WIMP capture rate similar to that from the previous chapter. It is worth highlighting that the two methods are very different: (1) The calculation in chapter 3 first computed the total probability of capture for every orbit and used that to produce a capture cross section. This cross section was then used in a numerical integration. (2) The second method starts with a random sample of initial WIMPs velocities, which is followed by an N-body simulation that models WIMP collisions and capture.

The fact that these two methods agree within a small factor helps to validate both simulations. It suggests that the simulations are fundamentally sound, in spite of the discrepancy with Scott et al. (2009). Ultimately, the purpose of this thesis is to compare the capture rate in a binary with that of a single star. Hence, what is needed is an N-body simulation that is sound, and can be used to compute the capture rate for single and binary stars.

Chapter 5

Binary system

Armed with a tested N-body code, it is time to proceed to the binary simulation. The code for the binary simulation is almost identical to the one that was tested in the previous chapter. The main changes include:

- The single star fixed at the origin is replaced by a binary system consisting of two stars of equal mass in a circular orbit centred at the origin. Later in this chapter there is a brief discussion of eccentric binaries.
- For a single star it is easy to only simulate orbits that cross the star, but in the binary case this is not easy. Hence, the binary simulation requires a much larger number of particles (100 times more) starting from much farther away. This means that the binary simulations also require far more CPU time (10 - 20 h per run).

5.1 Preliminary steps

5.1.1 Choice of binary configurations

The binary configurations used in this project were chosen to cover a range of stellar masses and binary separations, constrained by the computational time available to do the project. The orbital separations were chosen based on orbital speed rather than distance, since orbital speed is more physically meaningful in the context of this project:

$$\begin{aligned} M_\star &\in (1M_\odot, 3M_\odot, 5M_\odot, 10M_\odot, 30M_\odot) \\ v_{orb} &\in (20 \text{ km s}^{-1}, 35 \text{ km s}^{-1}, 50 \text{ km s}^{-1}, 80 \text{ km s}^{-1}, 110 \text{ km s}^{-1}, 140 \text{ km s}^{-1}) \\ \text{Orbital phase} &\in (0^\circ, 90^\circ) \end{aligned}$$

These parameters cover the range from high to low mass stars, and from wide to close orbits. For every choice of $M_\star$ and v_{orb} the simulation is run twice, with different orbital phases. This can help give us a sense of the margin of error in the simulations.

5.1.2 Initial WIMP orbits and collisions

However, the initial testing was done with the same ZAMS Sun from the previous chapters. To test the binary code I chose a wide binary of zero-age Sun-like stars, a described in Table 5.1.

Table 5.1: This is the configuration of the binary system used to test the N-body code. The wide binary and the zero-age Sun (ZAMS) is easier to compare with the earlier work with single stars. In this way, this binary is useful for validating the binary simulation.

Star A	$M = 1\ M_{\odot}$, ZAMS
Star B	$M = 1\ M_{\odot}$, ZAMS
Separation	200 $R_{\odot}$
Galactic orbital speed	220 km s^{-1}

This configuration was chosen because it is easiest to compare with the single-star simulation of the previous chapter: It uses the same stellar model, and it is easier to form an intuition about a wide binary. This preliminary test proved to be valuable because even this simulation showed a surprising result: Some WIMPs are scattered into complex orbits that make them cross a star at surprisingly low speeds.

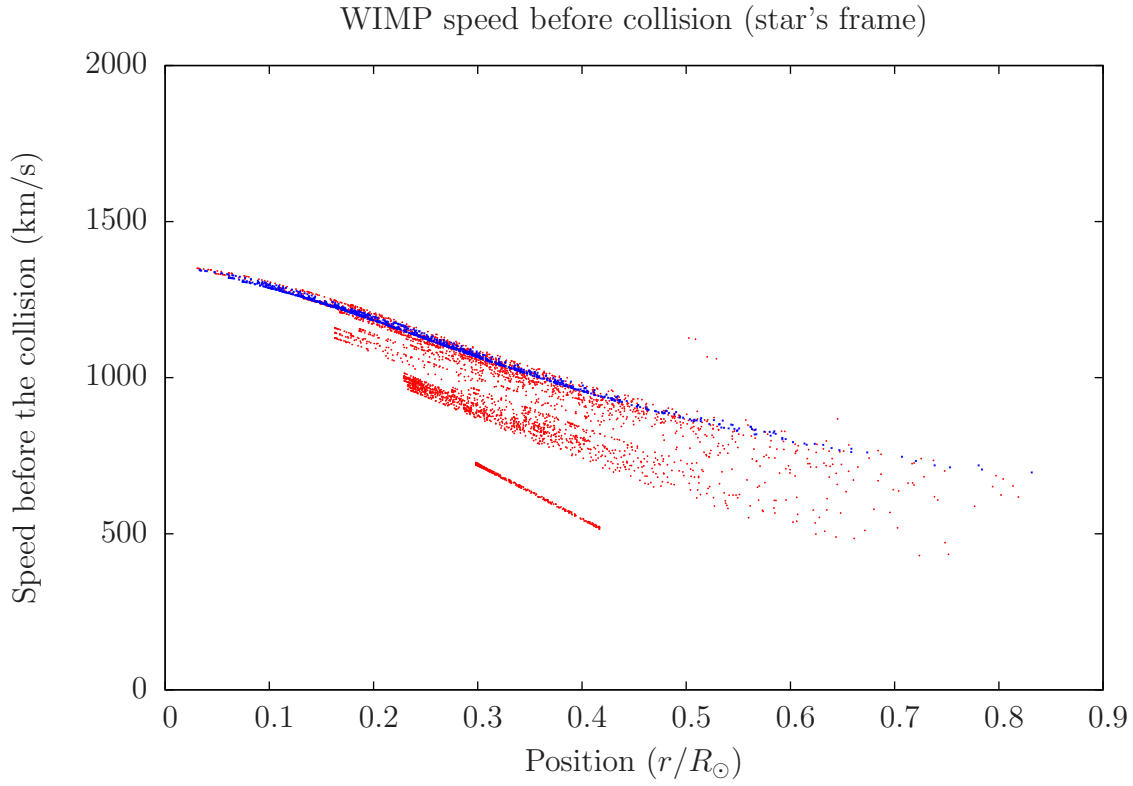

Figure 5.1: WIMP speed before a collision for a single star (blue) and a star in a binary (red). The binary system appears to have a large number of low-speed collisions. The reason why this occurs is made clear in Figure 5.2. As an aside: The binary data set covers nine WIMP orbits - recall that each WIMP orbit is allowed to scatter multiple times. This is necessary to ensure a large number of collisions with only modest computational work.

Figure 5.1 shows the speed of WIMPs at the moment they have a collision with a hydrogen atom. Notice that in the binary case there is a large number of collisions that occur at much lower speeds than in a single star. In fact, it even looks as if some WIMPs are already *captured* even before they have a collision.

A closer investigation revealed the cause for these low-speed collisions. Figure 5.2 shows the trajectory of one of the WIMP orbits responsible for the low-speed collisions. Notice that the WIMP is scattered into a complex orbit that includes a "*reverse gravitational slingshot*" with one of the stars, causing it to enter the second star in a slow, nearly co-orbital trajectory.

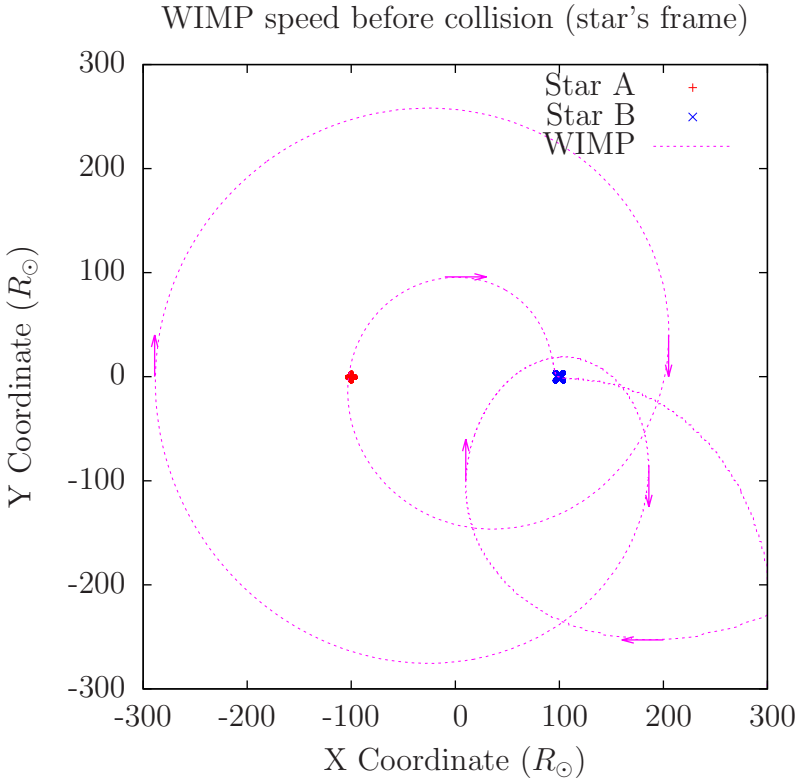

Figure 5.2: An example WIMP orbit in a binary system of zero-age Sun-like stars. The orbit is presented in the rotating reference frame of the binary. The WIMP enters the system at the bottom right corner, it has an encounter with star B which scatters the WIMP into an orbit around the binary. Eventually, the WIMP has a very close encounter with star A, *but does not go through star A*. This encounter is akin to a "*reverse gravitational slingshot*" which slows down the WIMP into a nearly co-orbital trajectory. Finally, the WIMP enters star B where it is gravitationally scattered out of the system. **Note**: There is no collision inside star B. The bent orbit is bent inside star B because stars are a distributed mass, so particles do not follow Keplerian orbits.

Satisfied that the WIMP orbits in a binary do look reasonable, it is time to proceed to the main results of this project.

5.2 Results

5.2.1 What does WIMP capture look like?

As shown in Figure 4.5, after the first collision WIMPs are scattered into highly eccentric orbits, with e usually higher than 0.975, and semi-major axis in the order of 0.1 to 1 AU. The aphelion is generally between 2 AU and 100 AU. Therefore, the binary separations examined in this project are certain to cause strong gravitational scatter of the WIMP orbits. The gravity of the two stars is likely to eject a large fraction of WIMPs before they have a chance to have a second collision that could bring the WIMP down to a more stable orbit. For this to happen, the WIMP has to cross the star about a few hundred times[1].

The upshot of this is that it turned out to be impractical to run a sufficiently large simulation for a sufficiently long period of time to directly measure a capture rate for any binary. Instead, it is necessary to infer properties of the capture rate from other quantities that are easier to measure:

- The number of WIMPs bound to the binary as a function of time[2].
- The number of WIMPs inside one of the Roche Lobes as a function of time.

These two quantities serve as upper bounds on the capture rate, and they will allow us to draw useful conclusions about WIMP capture in binaries. In addition, a closer look at the WIMP orbits inside the Roche Lobes will allow us to determine that the WIMP capture rate is effectively zero in binaries.

5.2.2 Limits on the capture rate

Figure 5.3 shows the evolution of one simulation ($M_\star = 1M_\odot$, $v_{orb} = 20\ \mathrm{km\ s^{-1}}$). The figure shows how WIMPs are quickly lost from the system, with only a small fraction surviving after 100 years. Furthermore, there is a clear trend of steady loss of WIMPs over the entire simulation. For this reason, the number of WIMPs bound or in a Roche Lobe after the 100 year simulation is probably a very conservative upper bound on the actual capture rate. This upper bound is shown in Figure 5.4 for $1M_\odot$ binaries and a range of orbital separations.

[1] This fact can be inferred from Figures 3.3 and 4.4 together. Figure 4.4 shows that about half of collisions in the single star simulation result in capture, and Figure 3.3 shows that for a low-speed WIMP, the probability of capture is typically 0.1% - 1%. Therefore, for a low-speed WIMP (which includes WIMPs in orbit) the probability of a collision is around 0.1% - 1% for each passing. Also, from Figure 4.3 we know that a collision removes $\sim 1\%$ of a WIMP's kinetic speed. One can calculate that a single collision can bring down the aphelion to $\sim 10R_\odot$.

[2] The reader may notice that there is no straight forward algebraic way to determine if a particle is bound to a binary system. For the purpose of this simulation, I have defined a WIMP as "*bound*" if one of the following conditions is true:

- The WIMP's distance to the origin is less than 5 times the binary separation.
- The WIMP is farther than 5 times the binary separation, **and** if we treat the binary as a point mass the WIMP has positive binding energy.

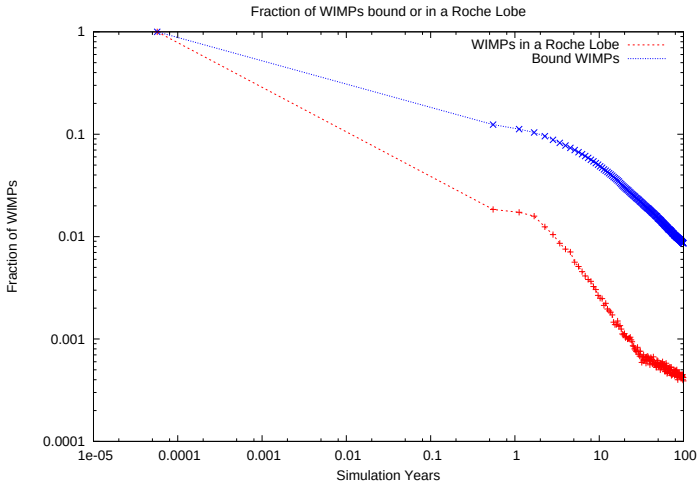

Figure 5.3: Evolution of one of the simulations ($M_\star = 1M_\odot$, $v_{orb} = 20$ km s^{-1}). This plot shows how the fraction of WIMPs that are bound, or in a Roche Lobe, decays quickly over time. After the first few decades of simulation time, the decay rate appears to stabilize as a straight line in the log-log plot.

Recall that for each value of $M_\star$ and v_{orb} the simulation is run twice, with each run having a different orbital phase. Therefore, the pairs of points in Figure 5.4 offer a rough indication on the margin of error in the simulations. As in chapter 4, the number of WIMPs bound (blue) or in a Roche Lobe (red) is converted to the equivalent capture rate in the Reference Solar Configuration (RSC). Figure 5.4 presents the same results twice: Once as capture rate versus orbital speed, and once as equivalent WIMP luminosity versus orbital separation.

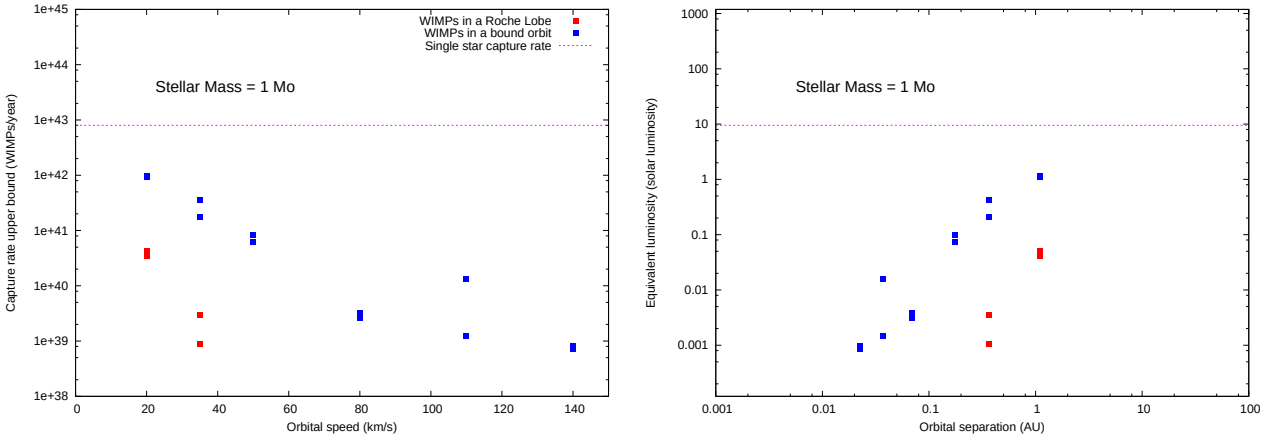

Figure 5.4: Upper bound on the capture rate based for a binary with $1M_\odot$ stars. The upper bound is calculated by assuming that after the 100 year simulation all the WIMPs that are bound (blue) or inside a Roche Lobe (red) will be captured by one of the stars. In these plots the capture rate is expressed as both WIMPs/year and as equivalent luminosity. The capture rate for a single star (N-body simulation from chapter 4) is also included for comparison.

The WIMP luminosity is derived from the capture rate: At some point in its life, a star will reach an equilibrium point between the capture and annihilation rates ($C = 2A$). Thus, if the capture rate is $C(n_\chi)$ WIMPs/year, for 100 GeV WIMPs that corresponds to a luminosity of $L = C(n_\chi) \times 100$ GeV/year minus a 10% energy loss to neutrinos (Scott et al., 2009). It is important to remember that the capture rate is computed in the Reference Solar Configuration

from Scott et al. (2009), and that the RSC probably has an unrealistic WIMP density (see section 3.5.1). Also remember that the N-body simulation may additionally overestimate the capture rate by a small factor (see section 4.2.1).

Figure 5.3 shows that, for one binary ($M_\star = 1M_\odot$, $v_{orb} = 20$ km s^{-1}) there are 100 times more "bound" WIMPs in year 0 than there are in year 100. Figure 5.4 shows that for the same binary, the number of bound WIMPs is about 10 times lower than for the single star case. This means that this simulation must have started with about 10 times more bound WIMPs than in the single star case. This suggests that stars in a binary do indeed have a greater collision cross section than single stars, but the WIMPs are quickly lost to gravitational scatter.

Finally, we turn our attention to the remaining simulations. Figure 5.5 shows the corresponding capture rate upper bounds for all the remaining simulations. It covers stellar masses from $3M_\odot$ to $30M_\odot$. The results are broadly consistent with those of Figure 5.4. Notice that more massive stars tend to have more WIMPs that are bound or in a Roche Lobe, though there is significant scatter. This is consistent with the findings of Scott et al. (2009).

Another observation regarding Figure 5.5 is that the widest orbits in the most massive star ($M_\star = 30M_\odot$) do not show the same downward trend in capture rate versus orbital separation that is so apparent in the other simulations. A partial explanation is that the widest orbit ($v_{orb} = 20$ km s^{-1}) corresponds to an orbital separation of around $a \sim 30$ AU, which may be wide enough to avoid the worst of the gravitational scatter. Another possible factor is that WIMP orbits are likely to be smaller for more massive binaries[3].

5.2.3 WIMP orbits inside a Roche Lobe

Figure 5.6 shows a sample WIMP orbit inside a Roche Lobe in the last year of simulation, after the chaotic period is past and the WIMP settles into a relatively stable orbit. The simulation corresponds to a wide binary of $1M_\odot$ stars with $v_{orb} = 20$ km s^{-1} ($a \approx 2.2$ AU). The orbit is shown along three planes (xy-plane, xz-plane, yz-plane) in the rotating reference frame where the two stars are fixed at $(x, y, z) = (\pm 119R_\odot, 0, 0)$. There is something very important to notice about this plot: *The WIMP orbit never crosses the star.* In fact, the WIMP orbit never reaches closer than about $\sim 5R_\odot$.

The orbit in Figure 5.6 is entirely typical of a WIMP in a Roche Lobe. The WIMP orbits vary in size, but a common feature is that they follow a Rosetta orbit that never crosses the star. This is significant because if a WIMP never crosses the star, it will never have a chance to have a second collision, and it will never be absorbed by the star. In other words, these orbits suggest that *the true capture rate for binary stars is essentially zero.*

We also observed from Figure 5.3 that the number of WIMPs inside a Roche Lobe decays steadily. These two observations together paint the following picture: Rather than being absorbed, WIMPs are captured into Rosetta orbits that never cross the star. Without crossing the star, there is no opportunity for further collisions, so the WIMPs remain in these orbits until gravitational interactions scatter the from the system entirely. This also suggests that it

[3]In a more massive star, the stellar core is much hotter, leading to more energetic WIMP-hydrogen collisions. Also, for a given orbit energy, an orbit around a $30M_\odot$ star will have a semi-major axis 30 times smaller than an orbit around a $1M_\odot$ star.

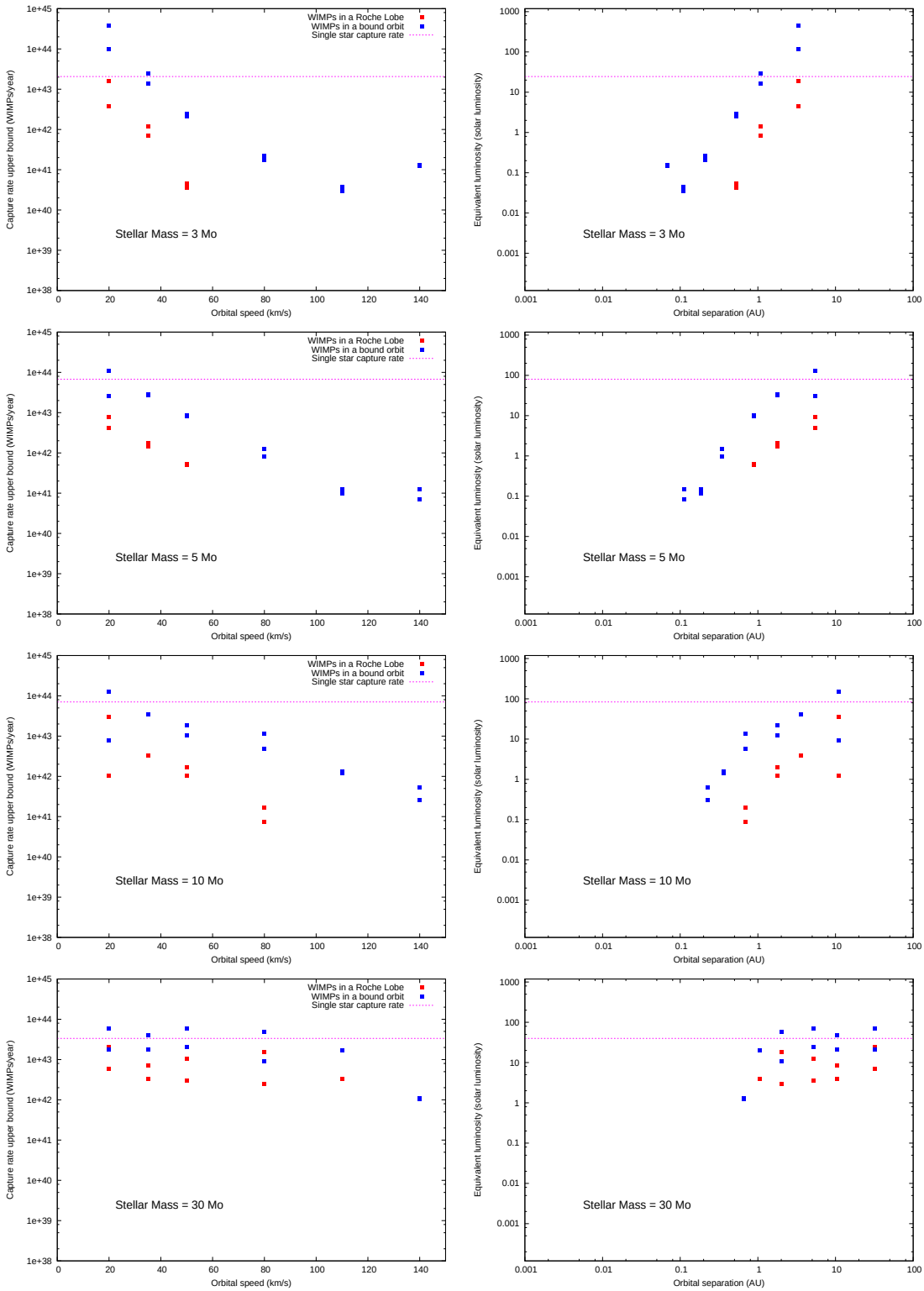

Figure 5.5: Capture rate upper bound for simulations with $3M_{\odot} \leq M_{\star} \leq 30M_{\odot}$. The upper bound is calculated by assuming that after the 100 year simulation all the WIMPs that are bound (blue) or inside a Roche Lobe (red) will be captured by one of the stars. In these plots the capture rate is expressed as both WIMPs/year and as equivalent luminosity. The capture rate for a single star (N-body simulation from chapter 4) is also included for comparison.

may be impractical to run a simulation large enough and long enough to measure the WIMP capture rate in a binary.

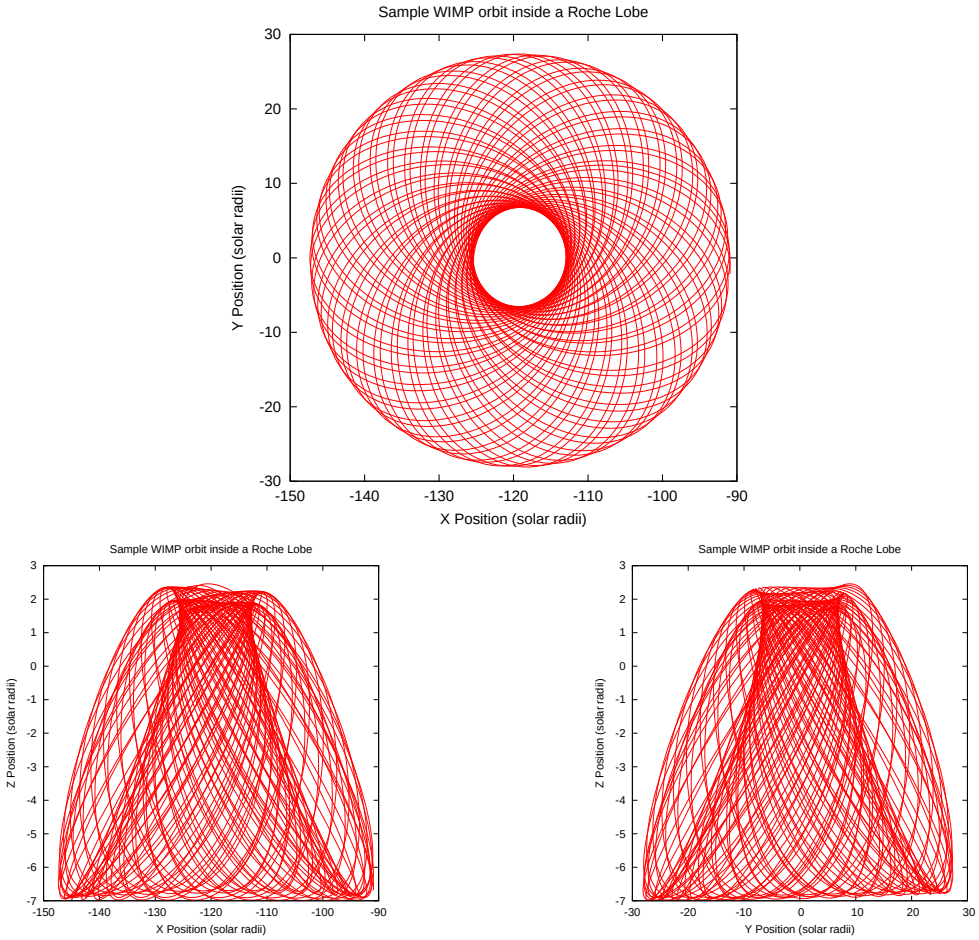

Figure 5.6: A typical example of a WIMP orbit inside a Roche Lobe in the last year of the simulation (after the WIMP has settled into a somewhat stable orbit). The binary configuration is $M_\star = 1M_\odot$, $v_{orb} = 20\,\mathrm{km\,s^{-1}}$ ($a \approx 2.2$ AU). The orbit is shown in the rotating reference frame where the star is fixed at $(x, y, z) = (-119R_\odot, 0, 0)$. The key observation is that the WIMP orbit never crosses the star. With no star crossings, there is no opportunity for the WIMP to be absorbed. This suggests that the capture rate in a binary may be essentially zero.

5.3 Additional discussion

The purpose of this section is to discuss points that are important or interesting, but which do not constitute actual *results* of the project.

5.3.1 Eccentric binaries

This project only modelled stellar binaries with circular orbits, but one can imagine a type of eccentric binary that could potentially have a much greater capture rate: The binary could have

a close, high-speed periapsis, with a large number of WIMP collisions, followed by a several hundred year orbit that allows those WIMPs to be fully absorbed before the next close stellar encounter.

What would this binary look like? For $1M_\odot$ stars, the periapsis would have to be no greater than about ~ 0.5 AU. The orbital period would have to be no less than around $T \sim 500$ years. Table 5.2 shows the orbital parameters for this binary.

Table 5.2: Orbital parameters for an eccentric binary of $1M_\odot$ stars with periapsis $r_p = 0.5$ AU and period $T = 500$ years.

Semi-major axis	$a = 62.97$ AU
Eccentricity	$e = 0.992$
Speed at periapsis	$v_p = 59.5$ km s^{-1}
Apoapsis	$r_{ap} = 97.08$ AU

With an eccentricity of $e = 0.992$, this kind of highly eccentric binary might exist, but is at least extremely rare. Hence, this type of binary is an unlikely target for observation.

5.3.2 Stars near the galactic centre

Is there any realistic orbit around the galactic centre that would be likely to capture enough WIMPs to contribute significantly to the star's luminosity? If the capture rate obtained in this project is correct, $\rho_\chi \sim 10^{10}$ GeV cm^{-3} (RSC) is roughly the minimum WIMP density needed for WIMP capture to contribute significantly to a star's luminosity. However, if there is indeed a scaling error and the correct capture rate is that found by Scott et al. (2009), this minimum WIMP density jumps to $\rho_\chi \sim 10^{13}$ GeV cm^{-3}. There are a couple of ways one could design an orbit near the galactic centre that maximize ρ_χ:

1. An orbit around the galactic super-massive black hole, where the star speed at apoapsis is low ($v_a \lesssim 220$ km s^{-1}) and periapsis is far enough to avoid losing WIMPs to the black hole (WIMP orbits remain within the star's Roche Lobe). Figure 4.5 shows that most WIMPs have $a \leq 100R_\odot$, so apoapsis is $r_a \leq 200R_\odot$. Thus, a Roche Lobe radius of $200R_\odot$ would contain most WIMP orbits.

2. Alternatively, one could design an orbit with $v_a = 220$ km s^{-1} and with an orbital period of around $T \sim 500$ years, to give WIMPs captured time to have a second collision before the star reaches periapsis.

The orbital parameters for these orbits and a $5M_\odot$ star are shown in Table 5.3, along with the WIMP density at apoapsis. The results suggest that even with the more optimistic WIMP density model, there probably aren't any orbits around the galactic centre with sufficient WIMP capture significantly contribute to a star's luminosity.

Table 5.3: Sample orbits for a $5M_\odot$ star near the galactic centre. These orbits aim to maximize WIMP capture using the WIMP density models from section 3.5.1. All scenarios fall far short of the $\rho_\chi \sim 10^{10}$ GeV cm^{-3} from the RSC. There appear to be no plausible orbits that can result in significant WIMP capture.

				$\rho_\chi(r_a)$ in GeV cm^{-3}	
Criterion	v_a	a	e	Model 1	Model 2
Roche Lobe $\geq 200R_\odot$	220 km s^{-1}	0.0125 pc	0.9319	1.1×10^5	9.8×10^7
Period $T = 500$ years	220 km s^{-1}	0.0485 pc	0.5416	3.3×10^4	1.8×10^7
Circular orbit	220 km s^{-1}	0.3554 pc	0	7.0×10^3	1.7×10^3

5.3.3 WIMP halo around binary stars

The WIMP orbits inside the Roche Lobes, as illustrated in Figure 5.6, suggest that stars in a binary system may be surrounded by a *halo* of WIMPs in Rosetta orbits. If this halo turned out to have a high enough WIMP density, it might be an interesting target for future observations seeking to detect direct WIMP-WIMP annihilation events. The simulations in this project only run for 100 years. They are far too short to make a meaningful estimate of the WIMP density around the stars. Hence, what follows is a *plausibility argument*, to evaluate whether these WIMP halos around binary stars could be an interesting target for future work.

Number of WIMPs in the halo

Figure 5.7 shows the fraction of WIMPs inside a Roche Lobe over the last 40 years of the $M_\star = 1M_\odot$, $v_{orb} = 20$ km s^{-1} simulation. The log-log plot shows a linear trend, which suggests that the number of WIMPs remaining inside the Roche Lobe drops with $N(t) \propto t^m$, where N is the number of WIMPs surviving in the Roche Lobe after time t.

$$\begin{aligned} \log\left(\frac{N(t)}{N_0}\right) &= m\log(t) + b \\ \Rightarrow \frac{N(t)}{N_0} &= C\,t^m \end{aligned}$$

If indeed $N(t)$ does not follow an exponential decay but is instead polynomial, there may never be an equilibrium point where the number of WIMPs entering and leaving the Rosetta orbits are equal. Instead, a polynomial relation suggests that a star will continue gathering WIMPs in its halo over its entire lifetime. To estimate the total number of WIMPs in the halo, it is best to think of $N(t)$ as the number of WIMPs that have been in an orbit for time t. In other words, the total number of WIMPs in the halo is:

$$\text{Total WIMPs} = \int_0^{T_{age}} N(t)\mathrm{d}t = \frac{C\,T_{age}^{m+1}}{m+1} \qquad \text{where } T_{age} \equiv \text{Age of the star} \tag{5.1}$$

Figure 5.7: Fraction of WIMPs inside a Roche Lobe over the last 40 years of the $1M_{\odot}$, $v_{orb} = 20$ km s^{-1} simulation. The log-log plot appears to have a linear trend, which suggests that the number of WIMPs remaining in the Roche Lobe drops with $N(t) \propto t^{m}$.

Figure 5.8 shows rough limits on C and m based on the same 40 year data set discussed earlier. Be aware that it is not at all reasonable to take a 40 year data set and extrapolate a trend over the 10-billion year age of a $1M_{\odot}$ star. The only purpose of this calculation is to show that WIMP halos may be an interesting target for additional study. Table 5.4 shows the number of WIMPs in the Roche Lobes based on the bounds from Figure 5.8.

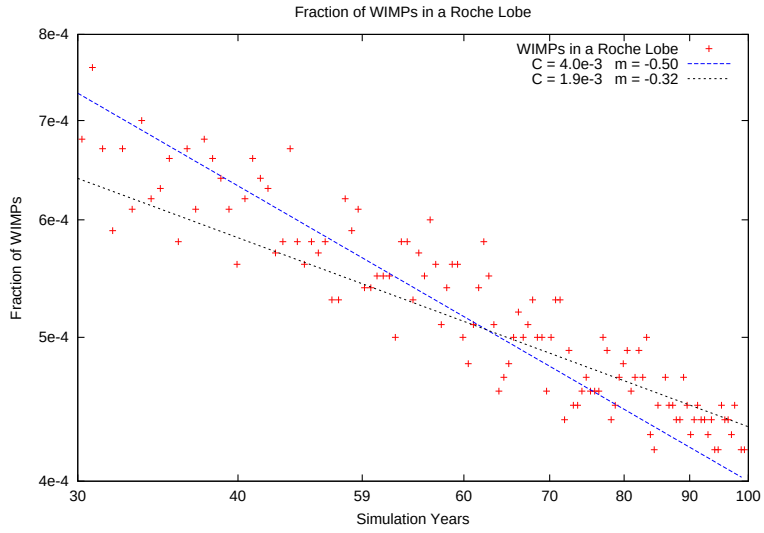

Figure 5.8: Fraction of WIMPs inside a Roche Lobe over the last 40 years of the $1M_{\odot}$, $v_{orb} = 20$ km s^{-1} simulation. The straight lines provide rough bounds on C and m from Equation 5.1. The blue line ($m = -0.5$) gives a lower limit on the number of WIMPs inside the Roche lobe, while the black line ($m = -0.32$) gives an upper limit.

All calculations up to this point have been in the "Reference Solar Configuration" (RSC) where $\rho_{\chi} \equiv 10^{10}$ GeV cm^{-3} and $v_{\star} = 220$ km s^{-1}. However, as noted in section 3.5.1, this does not correspond to any realistic orbit in the galaxy. For this reason, Table 5.4 is adjusted for the solar neighbourhood ($\rho_{\chi} \sim 1$ GeV cm^{-3}) and recreated in Table 5.5.

Table 5.4: Total number of WIMPs inside the Roche Lobes after 1 or 10 billion years. The lower bound is based on $C = 4 \times 10^{-3}$, $m = -0.5$ and the upper bound is based on $C = 1.9 \times 10^{-3}$, $m = -0.32$. These values are taken from Figure 5.8.

Binary age	Lower bound	Upper bound
10^9 years	2.5×10^{46}	3.7×10^{47}
10^{10} years	8.0×10^{46}	1.8×10^{48}

Table 5.5: This table has the values from Table 5.4 (number of WIMPs inside the Roche Lobes) adjusted for the WIMP density of the solar neighbourhood ($\rho_\chi \sim 1$ GeV cm^{-3}, see section 3.5.1).

Binary Age	Lower Bound	Upper Bound
10^9 years	2.5×10^{36}	3.7×10^{37}
10^{10} years	8.0×10^{36}	1.8×10^{38}

WIMP density

The Rosetta orbit in Figure 5.6 forms a fairly complex shape. Other WIMP orbits have a similar shape, but can vary in size. A very rough approximation is to describe the volume of these orbits as a torus with major radius $R \sim 16 R_\odot$ and minor radius $r \sim 10 R_\odot$. This torus has a volume of:

$$\text{Volume} = (\pi r^2)(2\pi R) = 1.06 \times 10^{37} \text{ cm}^3$$

With this, one can obtain the WIMP number and mass density, shown in Table 5.6. Notice that depending on the age of the binary and the assumed values of C and m, the WIMP density can be between $\sim 10^1$ and $\sim 10^4$ times greater than the ambient density.

Table 5.6: Depending on the age of the binary and the values of C and m (from Figure 5.8), the WIMP density around the stars is between $\sim 10^1$ and $\sim 10^4$ times greater than the ambient density (here, $\rho_\chi \sim 1$ GeV cm^{-3}). The WIMP-WIMP collision rate is calculated using the limit on the annihilation cross section from Calore et al. (2012).

Binary Age	Lower Bound	Upper Bound
10^9 years	2.5×10^{36} WIMPs	3.7×10^{37} WIMPs
	$n_\chi = 0.236$ cm^{-3}	$n_\chi = 3.491$ cm^{-3}
	$\rho_\chi = 23.6$ GeV cm^{-3}	$\rho_\chi = 349$ GeV cm^{-3}
10^{10} years	8.0×10^{36} WIMPs	1.8×10^{38} WIMPs
	$n_\chi = 0.755$ cm^{-3}	$n_\chi = 16.98$ cm^{-3}
	$\rho_\chi = 75.5$ GeV cm^{-3}	$\rho_\chi = 1698$ GeV cm^{-3}

The corresponding rate of WIMP-WIMP annihilations depends on the WIMP annihilation cross section σ_{an} which is currently poorly constrained. Calore et al. (2012) places an upper bound of $\langle \sigma_{an} v \rangle \leq 10^{-25}$ cm^{3}s^{-1}. For typical galactic velocities of $v \sim 200$ km s^{-1} that means $\sigma_{an} \sim 5 \times 10^{-33}$ cm^2. The WIMP orbits have speeds around $v \sim 109$ km s^{-1}. The total collision rate is $(v \sigma_{an} n_\chi) \times$ (Number of WIMPs). Table 5.7 shows the collision rate, as well as the photon flux that would be observed on Earth if the binary is 2 parsecs away and each WIMP annihilation produces a single gamma-ray photon. In all cases, the photon flux is far too small for a realistic detection.

Table 5.7: WIMP-WIMP collision rate inside the WIMP halos. The collision / annihilation cross section is taken from the upper limit from Calore et al. (2012). The photon flux corresponds to a binary 2 parsecs away, where each WIMP annihilation produces a single γ-ray photon. In all cases, the photon flux is too small for a realistic detection.

Binary Age		Lower Bound	Upper Bound
10^9 years	Collisions / second	3.2×10^{10}	7.0×10^{12}
	Flux on Earth (photons m^{-2} yr^{-1})	2.1×10^{-17}	4.6×10^{-15}
10^{10} years	Collisions / second	3.3×10^{11}	1.7×10^{14}
	Flux on Earth (photons m^{-2} yr^{-1})	2.2×10^{-16}	1.1×10^{-13}

The same calculation can be performed for a binary star close to the galactic centre. On the one hand, the binary will have many more WIMPs in the halo, but on the other, it will be more distant from Earth. The most optimistic orbit from Table 5.3 has an ambient density of $\rho_\chi \sim 10^8$ GeV cm^{-3}, or 10^8 times more than in the solar neighbourhood. Therefore, the collision rate is $(10^8)^2 = 10^{16}$ times greater than in the solar neighbourhood. But the galactic centre is $\sim 10,000$ pc away, or ~ 5000 times farther than the star considered in Table 5.7. This reduces the photon flux by a factor of $5000^2 = 2.5 \times 10^7$. All in all, this means that the γ-ray flux from a binary in the galactic centre is $\sim 4 \times 10^8$ times greater than for a nearby star (see Table 5.8), but still not enough to be detectable from Earth

Table 5.8: WIMP-WIMP collision rate inside the WIMP halos. The collision / annihilation cross section is taken from the upper limit from Calore et al. (2012). The photon flux corresponds to a binary near the galactic centre, where each WIMP annihilation produces a single γ-ray photon (compare with Table 5.7). Even in the best case scenario, the flux is too small for a realistic detection

Binary Age		Lower Bound	Upper Bound
10^9 years	Collisions / second	1×10^{19}	3×10^{21}
	Flux on Earth (photons m^{-2} yr^{-1})	9×10^{-7}	2×10^{-6}
10^{10} years	Collisions / second	1×10^{20}	1×10^{23}
	Flux on Earth (photons m^{-2} yr^{-1})	8×10^{-8}	4×10^{-5}

In other words, even in with the most optimistic assumption possible, of a binary near the galactic centre with zero extinction from the interstellar medium and a binary age of 10^{10} years, the photon flux at Earth would be no greater than 4×10^{-5} photons m^{-2} yr^{-1}. This flux is still far too small for any realistic detection from Earth.

5.4 Conclusions

- Binary stars capture significantly fewer WIMPs than single stars. The capture rate is too low to determine with the technique in this project, but the shape of WIMP orbits inside the Roche Lobes suggest that the capture rate may be approximately zero.
- The shape of WIMP orbits inside the Roche Lobe also indicates that stars in a binary system are surrounded by a WIMP halo. The simulations in this project are too short to estimate the WIMP density ρ_χ in the halo. However, a rough calculation suggests that ρ_χ might be between 10^1 and 10^4 times greater than the ambient density. However, the gamma-ray flux is unlikely to be detectable from Earth.

Chapter 6

Conclusions

This project was an attempt to bridge the gap between theoretical models of WIMP dark matter and direct astronomical observation. WIMPs, or Weakly Interacting Massive Particles, are a popular dark matter candidate, but their detection remains elusive. In an attempt to find concrete observational predictions, this project modelled the capture of WIMPs by single and binary stars.

In the process of developing a detailed model of how WIMPs interact with atoms, and how they are captured by stars, this report has made a number of interesting observations:

- WIMP capture is completely dominated by hydrogen. Perhaps contrary to intuition, this is not because hydrogen is the most common element inside stars. Rather, the dominant reason is that the weak-force mediated interaction between WIMPs and atomic nuclei can be divided into two distinct components: One set of interactions can only occur with nuclei that have a net quantum spin, while another set of interactions depends only on the atomic mass. As it turns out, the spin-dependent interaction has a much larger cross section σ_{SD} than the spin-independent interaction's cross section σ_{SI}. Hydrogen is the only common element in stars that has a net quantum spin.
- The probability that a collision between a WIMP and a nucleus will result in the WIMP being captured is determined by conservation of momentum. Some collisions simply cannot reduce the WIMP speed enough for the WIMP to become bound to the star. In general, as the temperature increases, a higher percentage of collisions can result in WIMP capture. For this reason, and also because of changes in density, the collision rate and the capture rate are dramatically higher in the inner regions of the star. Despite being a relatively small target, the stellar core is the main source of WIMP capture events.
- By the same token, for intermediate WIMP speeds ($v_\infty \sim 150$ km s^{-1}) there is a region of the star where collisions with hydrogen *never* result in WIMP capture. Furthermore, for initial WIMP speeds higher than $v_\infty \sim 200$ km s^{-1}, no collision with hydrogen, anywhere in the star, can result in a WIMP that is bound to the star. For these higher speed WIMPs, there will be a small number of capture collisions against more massive elements like oxygen, but the collision cross section of these elements is so small that they contribute a negligible amount to the total WIMP capture rate. In other words, for all intents and purposes, WIMPs travelling faster than $v_\infty \sim 200$ km s^{-1} in the reference frame of the star can be considered *non-capturable*.

Additional work using an N-body simulation revealed a more complete picture of WIMP capture in a single star: A collision with an atomic nucleus only removes $\sim 1\%$ of a WIMP's kinetic energy. As a result, the initial WIMP orbits are barely bound with very high eccentricities and apoapsis around ~ 5 AU. A second collision is required to bring the WIMP close to the star. As the probability of a collision is only around $\lesssim 1\%$, it normally takes several hundred orbits before a WIMP has that second collision.

The most challenging part of this project was the development of a sufficiently accurate N-body integrator. In particular, moving a particle through a distributed mass with a strong gravitational field is prone to numerical error. Also, even a nominally small error in energy of one part in 10^5 for each crossing becomes unacceptable after several hundred crossings. A Gragg-Bulirsch-Stoer integrator combined with a smooth polynomial approximation of the mass inside the star was found to be sufficiently accurate for this project.

The initial goal of this project was the study of WIMP capture in binary stars. Earlier work had shown that a star's ability to capture WIMPs is sensitive to the galactic speed of the star: A low stellar speed in the galactic reference frame translates into a star where WIMP speeds are lower in the *star*'s reference frame. This led to the hypothesis that a star in a binary system might have greater WIMP capture: A star in a binary would some times have a low speed in the galactic reference frame.

The work on binary systems indicates that binary stars do indeed start with a larger number of bound WIMPs than single stars. However, the vast majority of these WIMPs are quickly ejected from the system by gravitational scatter. The small fraction that survive for longer periods are placed into rosette type orbits around one of the stars. As these orbits do not cross the star, there is no opportunity for the WIMP to have a second collision and become absorbed by the star. Instead, the WIMP remains in the rosette orbit indefinitely, until the orbit precesses to the point that gravitational interactions scatter the WIMP entirely out of the system. As a result, the WIMP capture rate in binary stars is effectively zero.

The other implication of these WIMP orbits is that stars in a binary are surrounded by *WIMP halos*. The simulations in this project are insufficient to accurately measure the WIMP density in these halos. That said, the observed trend indicates that while these halos have a much higher WIMP density than the background, it is not high enough to directly detect WIMP annihilation from Earth.

Even for single stars, it is highly unlikely that any WIMP-burning star can be found anywhere in our galaxy. The highest WIMP density is found near the galactic super massive black hole. Scott et al. (2009) considered stars in very eccentric, very close orbits ($P \sim 10$ yr) around the black hole. The low speed at apoapsis, along with the high WIMP density, was thought to give maximal WIMP capture. However, this project shows that these orbits will not capture any WIMPs. WIMPs are initially bound in wide orbits with apoapsis ~ 5 AU. A close approach to the black hole within less than a few hundred years would cause the WIMP to be lost to the black hole before it can be fully absorbed by the star.

Appendix A

Analytic integration of the Form Factor

This section derives the analytic solution of $\int F(\Delta)\sin\theta d\theta$ using the approximation $\alpha = 0$ (Figure 2.2). If $\alpha = 0$, equations 2.5 and 2.6 become:

$$\begin{aligned} \boldsymbol{v}'_\chi &= \left[u\left(\frac{m_\chi}{m_N} + \cos\theta\right) + v_N\right]\hat{\boldsymbol{i}} + u\sin\theta\,\hat{\boldsymbol{j}} \\ u &= \mu_N(v_\chi - v_N) \end{aligned}$$

Where $\mu_N = \frac{m_N}{m_\chi + m_N}$ and $\mu_\chi = \frac{m_\chi}{m_\chi + m_N}$. To get the form factor, we need the energy loss Δ, and for that, we need v'^2_χ:

$$\begin{aligned} v'^2_\chi &= \left[u\left(\frac{m_\chi}{m_N} + \cos\theta\right) + v_N\right]^2 + u^2\sin^2\theta \\ &= u^2\left(\frac{m_\chi}{m_N} + \cos\theta\right)^2 + 2\,u\,v_N\left(\frac{m_\chi}{m_N} + \cos\theta\right) + v_N^2 + u^2\sin^2\theta \\ &= u^2\left(\left(\frac{m_\chi}{m_N}\right)^2 + 1\right) + 2\,u^2\,\frac{m_\chi}{m_N}\cos\theta + 2\,u\,v_N\left(\frac{m_\chi}{m_N} + \cos\theta\right) + v_N^2 \\ &= u^2\left(\left(\frac{m_\chi}{m_N}\right)^2 + 1\right) + 2\,u\,v_N\frac{m_\chi}{m_N} + v_N^2 + 2\cos\theta\left(u^2\frac{m_\chi}{m_N} + u\,v_N\right) \end{aligned}$$

Now we are ready to calculate the energy loss:

$$v_\chi^2 - v'^2_\chi = (v_\chi^2 - v_N^2) - u^2\left(\left(\frac{m_\chi}{m_N}\right)^2 + 1\right) - 2\,u\,v_N\frac{m_\chi}{m_N} - 2\cos\theta\left(u^2\frac{m_\chi}{m_N} + u\,v_N\right)$$

Substitute $u = \mu_N(v_\chi - v_N)$ and let $w \equiv \frac{v_N}{v_\chi}$:

$$\begin{aligned}\Delta &\equiv \frac{v_\chi^2 - v_\chi'^2}{v_\chi^2} \\ &= 1 - w^2 - \mu_N^2(1-w)^2\left(\left(\frac{m_\chi}{m_N}\right)^2 + 1\right) - 2\mu_N(1-w)w\frac{m_\chi}{m_N} \\ &\quad -2\cos\theta\left(\mu_N^2(1-w)^2\frac{m_\chi}{m_N} + \mu_N(1-w)w\right)\end{aligned}$$

Using $\mu_N\frac{m_\chi}{m_N} = \mu_\chi$, the above simplifies to:

$$\begin{aligned}\Delta &= 1 - w^2 - (1-w)^2\left(\mu_\chi^2 + \mu_N^2\right) - 2\mu_\chi(1-w)w \\ &\quad -2\cos\theta\mu_N\left[\mu_\chi(1-w)^2 + w(1-w)\right]\end{aligned}$$

With a little algebra one can show $\mu_\chi^2 + \mu_N^2 = 1 - 2\mu_\chi\mu_N$, giving:

$$\begin{aligned}\Delta &= 1 - w^2 - (1-w)^2(1-2\mu_\chi\mu_N) - 2\mu_\chi(1-w)w \\ &\quad -2\cos\theta\mu_N\left[\mu_\chi(1-w)^2 + w(1-w)\right] \\ &= 1 - w^2 - 1 + 2w - w^2 + 2(1-w)^2\mu_\chi\mu_N - 2\mu_\chi(1-w)w \\ &\quad -2\cos\theta\mu_N(1-w)[\mu_\chi(1-w) + w] \\ &= 2w(1-w) + 2(1-w)^2\mu_\chi\mu_N - 2\mu_\chi(1-w)w \\ &\quad -2\cos\theta\mu_N(1-w)[\mu_\chi - \mu_\chi w + w] \\ &= 2w(1-w) + 2\mu_\chi(1-w)[\mu_N(1-w) - w] \\ &\quad -2\cos\theta\mu_N(1-w)[\mu_\chi - \mu_\chi w + w] \\ &= 2\mu_\chi(1-w)[\mu_N - \mu_N w - w + \frac{w}{\mu_\chi}] \\ &\quad -2\cos\theta\mu_N(1-w)[\mu_\chi - \mu_\chi w + w] \\ &= 2\mu_\chi(1-w)[\mu_N + w(\frac{1}{\mu_\chi} - \mu_N - 1)] \\ &\quad -2\cos\theta\mu_N(1-w)[\mu_\chi + w(1-\mu_\chi)]\end{aligned}$$

This can be simplified further by noting that $\mu_\chi + \mu_N = 1$. Therefore, $w(1-\mu_\chi) = w\mu_N$, and:

$$
\begin{aligned}
w(\frac{1}{\mu_\chi} - \mu_N - 1) &= w(\frac{1 - \mu_N\mu_\chi - \mu_\chi}{\mu_\chi}) \\
&= w(\frac{(1-\mu_\chi) - \mu_N\mu_\chi}{\mu_\chi}) \\
&= w(\frac{\mu_N - \mu_N\mu_\chi}{\mu_\chi}) \\
&= w(\frac{\mu_N(1-\mu_\chi)}{\mu_\chi}) \\
&= w(\frac{\mu_N\mu_N}{\mu_\chi})
\end{aligned}
$$

Thus, the energy loss equation simplifies to:

$$
\begin{aligned}
\Delta &= 2\mu_\chi(1-w)[\mu_N + w\ \frac{\mu_N\mu_N}{\mu_\chi}] \\
&\quad -2\cos\theta\mu_N(1-w)[\mu_\chi + w\mu_N] \\
&= 2\mu_\chi\mu_N(1-w)[1 + w\ \frac{\mu_N}{\mu_\chi}] \\
&\quad -2\cos\theta\mu_N(1-w)[\mu_\chi + w\mu_N] \\
&= 2\mu_N(1-w)[\mu_\chi + w\mu_N] \\
&\quad -2\cos\theta\mu_N(1-w)[\mu_\chi + w\mu_N]
\end{aligned}
$$

Now we can write:

$$
\begin{aligned}
A &= 2\mu_N(1-w)(\mu_\chi + w\mu_N) \\
\therefore \Delta &= A(1-\cos\theta)
\end{aligned}
$$

Now we are ready to calculate the form factor $F(\Delta) = \exp(\frac{-E_\chi}{E_0}\Delta)$:

$$
\begin{aligned}
B &= \frac{E_\chi}{E_0}A \\
F(\Delta) &= e^{B(\cos\theta - 1)}
\end{aligned}
$$

We can now integrate this analytically:

$$
\int_0^\pi F(\Delta)\ \sin\theta\ d\theta = \frac{1 - e^{-2B}}{B}
$$

Bibliography

Abbasi, R. et al. 2009, Physical Review Letters, 102, 201302, 0902.2460

Ahmed, Z. et al. 2009, Physical Review Letters, 102, 011301, 0802.3530

Amanullah, R. et al. 2010, ApJ, 716, 712, 1004.1711

Anders, E., & Grevesse, N. 1989, Geochim. Cosmochim. Acta, 53, 197

Angle, J. et al. 2008, Physical Review Letters, 100, 021303, 0706.0039

Armengaud, E. et al. 2010, Physics Letters B, 687, 294, 0912.0805

Behnke, E. et al. 2008, Science, 319, 933, 0804.2886

Bernabei, R. et al. 2008, European Physical Journal C, 56, 333, 0804.2741

Bertone, G. 2010, Nature, 468, 389, 1011.3532

Braun, J., Hubert, D., & for the IceCube Collaboration. 2009, ArXiv e-prints, 0906.1615

Brayeur, L., & Tinyakov, P. 2011, ArXiv e-prints, 1111.3205

Calore, F., de Romeri, V., & Donato, F. 2012, Phys. Rev. D, 85, 023004, 1105.4230

CDMS II Collaboration et al. 2010, Science, 327, 1619, 0912.3592

Chakraborti, S., & Khedekar, S. 2011, ArXiv e-prints, 1109.0529

Desai, S. et al. 2004, Phys. Rev. D, 70, 083523, arXiv:hep-ex/0404025

Diemand, J., Kuhlen, M., & Madau, P. 2007, ApJ, 657, 262, arXiv:astro-ph/0611370

Dodelson, S. 2011, ArXiv e-prints, 1112.1320

Eggleton, P. P. 1971, MNRAS, 151, 351

Evans, A. 2010, amateur photo of M31, under the Creative Commons Attribution 2.0 license. http://www.flickr.com/photos/astroporn/4999978603/

Feng, J. L. 2010, ARA&A, 48, 495, 1003.0904

Gustafsson, M., Fairbairn, M., & Sommer-Larsen, J. 2006, Phys. Rev. D, 74, 123522, arXiv:astro-ph/0608634

Hamerly, R., & Kosovichev, A. 2011, ArXiv e-prints, 1110.1169

Jungman, G., Kamionkowski, M., & Griest, K. 1996, Phys. Rep., 267, 195, arXiv:hep-ph/9506380

Kim, Y. G., Nihei, T., Roszkowski, L., & Ruiz de Austri, R. 2002, Journal of High Energy Physics, 12, 34, arXiv:hep-ph/0208069

Krauss, L. M., Freese, K., Spergel, D. N., & Press, W. H. 1985, ApJ, 299, 1001

Lebedenko, V. N. et al. 2009, Phys. Rev. D, 80, 052010, 0812.1150

Lee, H. S. et al. 2007, Physical Review Letters, 99, 091301, 0704.0423

Milgrom, M. 1983, ApJ, 270, 365

Moore, B., Ghigna, S., Governato, F., Lake, G., Quinn, T., Stadel, J., & Tozzi, P. 1999, ApJ, 524, L19, arXiv:astro-ph/9907411

Moroi, T., & Nakayama, K. 2011, ArXiv e-prints, 1112.3123

Navarro, J. F., Frenk, C. S., & White, S. D. M. 1996, ApJ, 462, 563, arXiv:astro-ph/9508025

Navarro, J. F. et al. 2004, MNRAS, 349, 1039, arXiv:astro-ph/0311231

Olive, K. A., Steigman, G., & Walker, T. P. 2000, Phys. Rep., 333, 389, arXiv:astro-ph/9905320

Pols, O. R., Tout, C. A., Eggleton, P. P., & Han, Z. 1995, MNRAS, 274, 964, arXiv:astro-ph/9504025

Press, W. H., & Spergel, D. N. 1985, ApJ, 296, 679

Press, W. H., Teukolsky, S. A., Vetterling, W. T., & Flannery, B. P. 2002, Numerical recipes in C++ : the art of scientific computing (Cambridge University Press)

Primack, J. R. 2001, ArXiv Astrophysics e-prints, arXiv:astro-ph/0112336

Ressell, M. T., Aufderheide, M. B., Bloom, S. D., Griest, K., Mathews, G. J., & Resler, D. A. 1993, Phys. Rev. D, 48, 5519, arXiv:hep-ph/9307228

Rubin, V. C., & Ford, Jr., W. K. 1970, ApJ, 159, 379

Scott, P., Fairbairn, M., & Edsjö, J. 2009, MNRAS, 394, 82, 0809.1871

Spergel, D. N., & Press, W. H. 1985, ApJ, 294, 663

Taoso, M., Bertone, G., & Masiero, A. 2008, JCARASC, 3, 22, 0711.4996

Trotta, R., Feroz, F., Hobson, M., Roszkowski, L., & Ruiz de Austri, R. 2008, Journal of High Energy Physics, 12, 24, 0809.3792

Zwicky, F. 1933, Helvetica Physica Acta, 6, 110